Quantitative Approaches to the Cancer Stem Cell Hypothesis

by

Seyed Ali Madani Tonekaboni

A thesis
presented to the University of Waterloo
in fulfillment of the
thesis requirement for the degree of

Master of Mathematics
in
Applied Mathematics

Waterloo, Ontario, Canada, 2015

AUTHOR'S DECLARATION

I hereby declare that I am the sole author of this thesis. This is a true copy of the thesis, including any required final revisions, as accepted by my examiners.

I understand that my thesis may be made electronically available to the public.

Abstract

In this thesis, phenotype switching in cancer cell populations is modeled. We focus on the behavior of cells at the phenotypic level and present mathematical models to capture the results of available experiments. The models, based on the cancer stem cell hypothesis (in addition to the new concept of plasticity in tumor populations), are also employed to predict cancer cell growth *in vitro* and *in vivo*.

The models are analyzed in the two limits of large and small cell numbers. We use stochastic analysis to capture the random behavior of cells in the limit of low number as observed in mammosphere formation assays (MFAs). Stochastic analysis is employed to estimate quantities such as survival rate while the deterministic solution of the models is obtained to simulate the average behavior of cells. The importance of stochastic analysis and deterministic simulations is discussed in detail.

The primary purpose of the thesis is to highlight the importance of stochastic analysis in cancer stem cell experiments. The models are developed or modified based on the idea that both stochastic and deterministic behavior of cells should be considered simultaneously. In order to describe the behavior of the cells in cancer stem cell assays, the developed models are then used to investigate the possible experimental errors in the area and suggest possible filtration methods for corresponding experiments. In addition, the models are used to investigate the behavior of tumors under radiotherapy; and the effects of phenotype switching on the efficiency of therapies are investigated in the final part of the thesis.

Acknowledgements

The chapters presented in this thesis are based on the projects and papers to which I have contributed during the period of my Master's degree in the Biomedical Research Group. Prof. Mohammad Kohandel as my supervisor and Andrew Dhawan as my colleague helped me finish the projects and the papers. The financial support for my study has been provided by the University of Waterloo and an NSERC grant. The Ping Yang award also helped me to go to the US and present my projects at UC Berkeley and the University of Illinois at Urbana Champaign.

I'd like to thank my supervisor, Prof. Kohandel, and Prof. Sivaloganathan for their support, in addition to the opportunities they have given me and the lessons they have taught me.

In addition to the projects presented as different chapters of this thesis, I have done two other projects which was not exactly in the direction of this thesis. Both of themare currently under review. The first paper focuses on the synergetic behavior of glutathione peroxidase and peroxiredoxin family in the cellular environment. This project was done in collaboration with Dr. Hamid Molavian. The paper models the effect of hypoxia on the population of breast cancer cells *in vitro*. It has been prepared in collaboration with Prof. Mani's group at MD Anderson Cancer Centre, Texas and Andrew Dhawan, a previous student in our group. I'd like to thank Dr. Joseph Taube and Dr. Aaron Goldman who helped me in these projects by providing experimental data.

Dedication

I’d like to dedicate this thesis to my parents, my brother, and my love and thanks to them for the unwavering and universal support they’ve given me.

Table of Contents

List of abbreviations

ABBREVIATION	FULL STATEMENT
CSC	Cancer stem cell
MFA	Mammosphere formation assay
MFE	Mammosphere formation efficiency
TCM	Two compartment model
AMS	Average mammosphere size
SFA	Sphere formation assay
SFE	Sphere formation efficiency
ASPS	Average sphere size
NFE	Neurosphere formation efficiency
PMCM	Proliferative-migratory model

List of Figures

List of Tables

Chapter 1
Introduction

1.1 What is cancer?

Cells are the building blocks of our tissues and organisms. Our body includes organs, each of which contains different tissues, and cells are the building blocks of these tissues. Cells grow in a controlled way so that the size of the tissue and its structure remains at a controlled normal level. The cells divide and die in order to maintain equilibrium in our body. However, losing this equilibrium, causes abnormal growth of the cells, which is called cancer. The extra mass of cells aggregates in a tissue is called a tumor, and this can be benign or malignant.

1.1.1 Benign tumors

Benign tumors are not usually a threat to life. They can be removed in most cases and do not have the capability of spreading to other parts of the body and developing tumors in other tissues. Some examples of benign tumors are presented in Table 1.

Table 1 Examples of benign tumor types and a brief description of their characteristics.

Name	Description
Adenoma	Grows in and around the glands
Osteoma	Originating in the bones
Angioma	Usually composed of small blood vessels
Lipoma	A tumor in a fatty tissue

1.1.2 Malignant tumors

Unlike benign tumors, malignant tumors can invade and damage the nearby tissues. They also have the ability to spread to other parts of the body using the lymphatic or vascular system in a process called metastasis. They can grow in secondary locations and develop new tumors. Some of the important types of malignant tumors (or cancer) are presented in Table 2.

Table 2 Examples of malignant tumor types and a brief description of their characteristics.

Type	Description
Carcinoma	Originating from epithelial cells (most cancer are carcinomas)
Sarcoma	Originating from bone, fat muscle or connective tissues
Leukemia	Malignant white blood cells
Lymphoma	Altered lymphatic system cells
Myelomas	Results from changes in specialized white blood cells that make antibodies

Cancer can be caused by environmental factors like chemicals, tobacco and ionizing radiation. These factors cause genetic alterations and, subsequently, epigenetic changes result in cancer cells in a tissue.

1.2 The hallmarks of cancer

The hallmarks of cancer (Fig. 1) are the physiological characteristics or potentials that underlie different cancer cells and tumor types [1]. However, some tumor types or a tumor at different stages of its development may not show all of these features, e.g. metastasis may not operate at the early stages of tumor growth. Acquiring knowledge about the hallmarks of cancer can help to estimate the behavior of tumors and to find appropriate therapies (Fig. 1).

Initially, it was believed that tumors were homogeneous and the result of the evolution of a single phenotype. However, it is now widely accepted that any tumor includes different phenotypes. The well-known cancer stem cell (CSC) hypothesis has helped scientists in the field to explain this heterogeneity [2]. The cells in tumors may be phenotypically heterogeneous because of being in different stages of differentiation [1]. We will discuss the CSC hypothesis in detail later in this chapter.

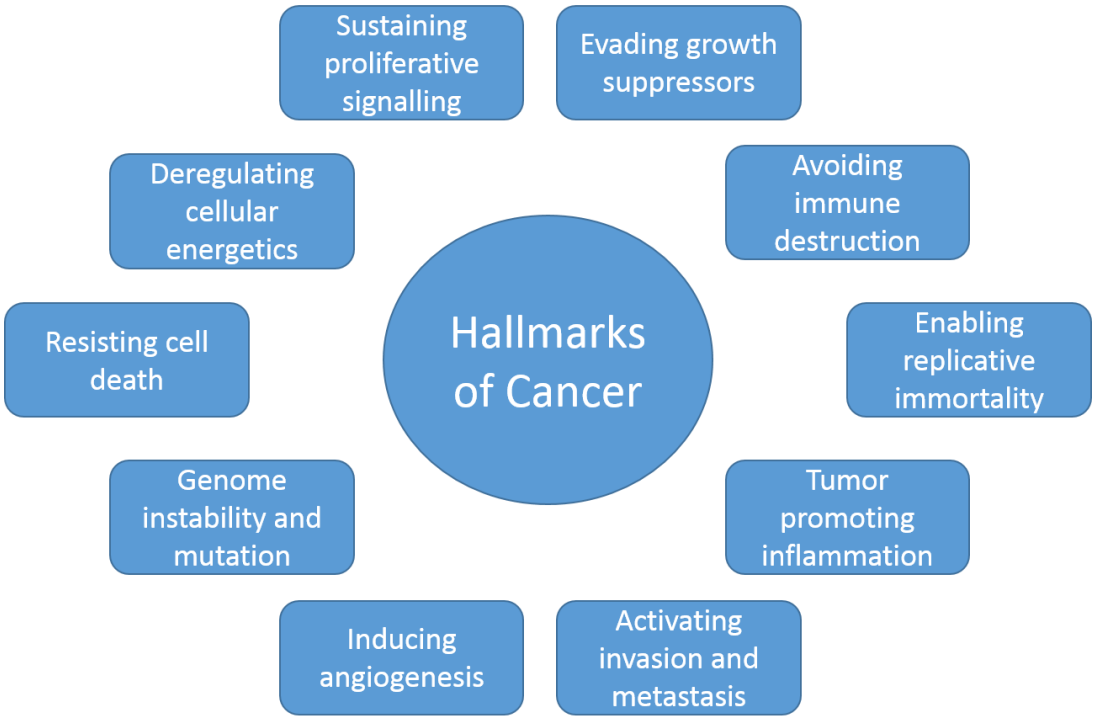

Figure 1 "Therapeutic targeting of the hallmarks of cancer"(reproduced from [1]).

1.3 Hypotheses

The basic hypotheses of theories of tumor cell phenotypes and their growth has evolved over the last fifty years of research in the field. Here, we briefly introduce three main ideas: **Clonal Evolution**, **Cancer Stem Cell Hypothesis**, and **Tumor Plasticity**.

Clonal Evolution: Most tumors arise from single cells through the sequential accumulation of numerous genetic changes and epigenetic modifications.

Cancer Stem Cell Hypothesis [2]**:** Only "cancer initiating cells" have the capacity for unlimited proliferation and are therefore responsible for the initiation and maintenance of tumors.

In order to clarify the differences of these two models, the assumptions and the subsequent conclusions of the models are presented in Table 3.

Table 3 Comparison of CSC and Clonal Evolution models.

	Cancer Stem Cell Model	Clonal Evolution
Frequency of cancer cells with tumorigenic potential	**Rare to Moderate**	**High**
Phenotype of cancer cells	**Heterogeneous**	**Heterogeneous or Homogeneous**
Tumor organization	**Hierarchical**	**Not hierarchical**
Rational approach to therapy	**Target only tumorigenic cells**	**Target most or all cells**

The CSC hypothesis was originally proposed because of the similarity between some of the properties of stem cells in normal tissues and these phenotypes in tumors (Table 4 and 5).

Table 4 Comparison of normal and cancer stem cells.

Normal stem cells	Rare cells within organs with the ability to self-renew and give rise to all types of cells within the organ to drive organogenesis.
Cancer stem cells	Rare cells within tumors with the ability to self-renew and give rise to the phenotypically diverse tumor cell population to drive tumorigenesis.

Recently a new concept has emerged in the field of cancer biology, which could be also considered a new hypothesis.

Tumor Plasticity: A degree of plasticity between the non-CSC and CSC compartments may exist in cancer cell populations (Fig. 2).

Table 5 Examples of similarities between normal and cancer stem cells.

Self-renewal toward generating two cells of the same phenotype as the cells of origin.
• Tissue-specific stem cells must self-renew to maintain specific organs. • Cancer stem cells undergo self-renewal to maintain tumor growth.
Differentiation into phenotypically diverse mature cell types.
Give rise to a heterogeneous population of cells of which the organ or tumor is composed but lack the ability for unlimited proliferation (hierarchical arrangement of cells).
Regulation by similar pathways
Pathways that regulate self-renewal in normal stem cells are also regulated in cancer stem cells.

The existence of plasticity means that targeting only CSCs in each tumor may not be the solution and that the non-CSCs may dedifferentiate generating more CSCs.

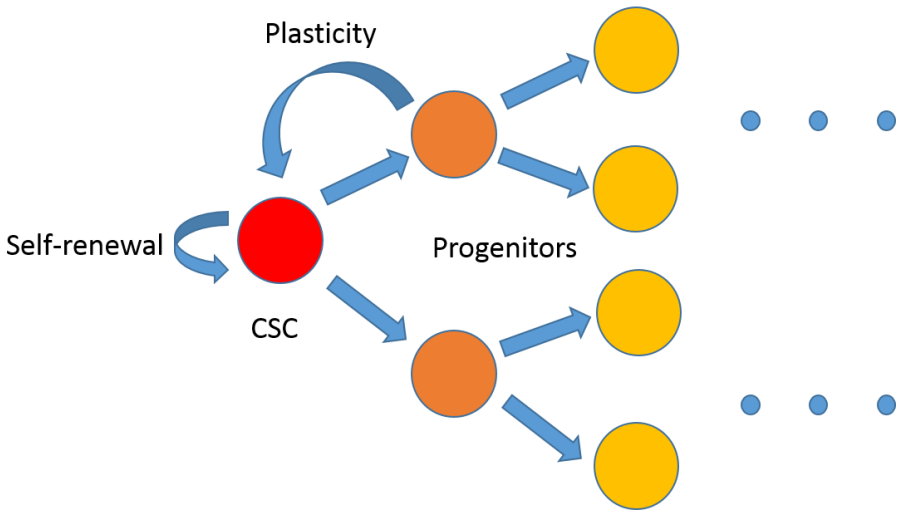

Figure 2 "Stem-differentiation hierarchy. Increased plasticity may be present within cancer populations, enabling bidirectional interconvertibility between CSCs and non-CSCs" (reproduced from [3]**).**

1.4 Tumor microenvironment

One of the factors that dynamically affects the behavior of cancer cells *in vivo* is the tumor microenvironment. Oxygen concentration and pH level are among the important parameters in the tumor microenvironment that affect the behavior of cells and vary the growth rate and aggressiveness of tumors [4]. It has been shown that hypoxia, a low concentration of oxygen, reduces the lethal effect of radiotherapy [4]. Hypoxia may cause the cells to go to a resistant state and not to show the expected behavior under radiation therapy and chemotherapy.

Hypoxia may cause switching between the phenotypes, resulting in more CSCs in the population [5]. Proliferation capacity, self-renewal and tumorigenicity of cancer cells in hypoxic regions can be increased [6]. Higher tumoreginic potential and resistance in hypoxia make it a harsh microenvironment for the tumors. Acidity may also have the same effect [7].

1.5 Mathematical models

In general, two types of mathematical models have been proposed based on the biological hypotheses of tumor growth: **hierarchical** and **phenomenological**. In the hierarchical models, we consider a hierarchy of cells similar to the hierarchy of normal cells originating from stem cells [8] (Fig. 3 (a)) while in phenomenological models we do not want to exactly simulate the hierarchy of differentiation in cancer cell populations. We consider similar phenotypes of cancer cells in one compartment in the phenomenological models (for example we can consider two compartment of CSCs and non-CSCs as shown in Fig. 3 (b)).

In both kind of models, other concepts can be added, such as the imperfectness of surface biomarkers [8] used in the experiments to recognize CSCs and other phenotypes in the population of cancer cells.

1.5.1 Mathematical analysis

We can analyze the behavior of cancer cells in the two limits of small and large populations. In each model, small populations of cells can be analyzed using stochastic modeling, and large populations can be modeled deterministically [9], [10].

In stochastic modeling of the tumor cells, we capture random behavior of cells and try to understand the behavior of single cells. On the other hand, deterministic analysis gives us the average behavior of cells and is useful when we are dealing with large cell populations. The importance of stochastic analysis is discussed in detail in the next chapters.

There are some experiments or biological terminology that are described in the next chapters.

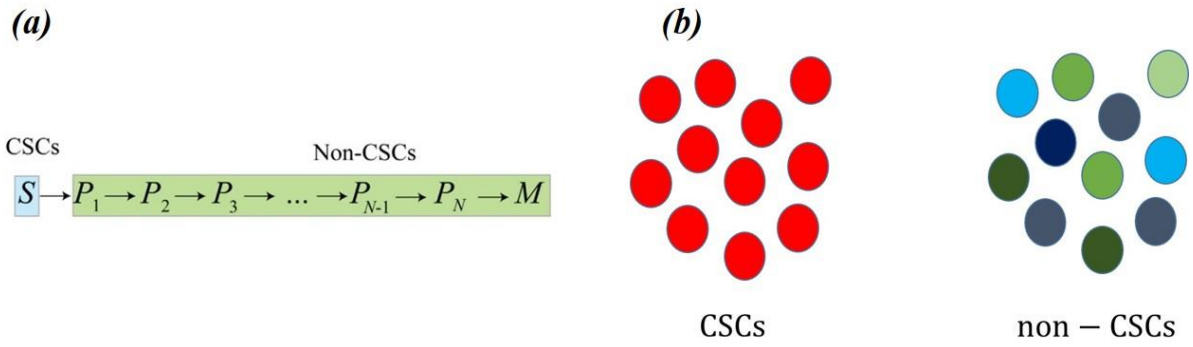

Figure 3 Schematic representation of (a) a hierarchical model (*S* is used to show CSC and P_i are generations of non-CSCs and *M* is the mature cell in the last stage of the hierarchy) and (b) a phenomenological model (red spheres are CSCs and the other colors are other phenotypes in the modeled tumor).

1.6 Order of chapters

We describe four projects that investigate the behavior of cancer cell populations based on the CSC hypothesis. In the first chapter, we suggest that deterministic analysis is not enough to capture the behavior of cancer cells and stochastic modeling should be also taken into consideration. To show the importance of stochastic analysis, a phenomenological model, two-compartment model, and a hierarchical model are used. We also discuss in the second chapter how the experimental errors in cancer studies can be included in the modeling. We use this concept and propose a new model in chapter three to show the importance of imperfectness of biomarkers in cancer study. In addition, we briefly discuss possible errors in mammosphere formation assays (MFA). Then, we use the modeling in chapter four to analyze and show the importance of these errors in MFA. Finally, the last chapter is dedicated to the effect of switching between different phenotypes in tumor populations when radiotherapy is applied.

Chapter 2

Plasticity and phenotype switching in cancer cell populations: stochastic versus deterministic approaches

The traditional view of tumor growth is based on the hypothesis of monoclonal cellular expansion. The alternative cancer stem cell hypothesis suggests that only a subpopulation of so-called cancer stem cells (CSCs) has the capacity to proliferate via a hierarchical model of unidirectional differentiation. However, growing experimental evidence suggests the existence of a bidirectional hierarchy, in which dedifferentiation of cancer cells toward CSCs is permitted. Various mathematical models have been developed over the past few years enabling the incorporation of plasticity and phenotype switching in cancer cell populations. The focus of most of these models and analysis is on the behavior of the cancer cells in the limit of a large population. However, the behavior of these models changes in the limit of small numbers of cells, which correlates with biologically relevant assays such as the mammosphere formation assay (MFA), in which stochastic effects predominate. We show that the stochastic behavior of cancer cells with the same deterministic compartment, defined as the average of random behavior of single cells, can be extremely different. We also explore the potential effect of plasticity acting to decrease the survival probability of cancer stem cells stochastically, while still increasing survival in the large population analysis. Conclusively, we show that both small and large populations of cancer cells should be studied at the same time to be able to propose a promising model.

2.1 Introduction

Heterogeneity among cellular populations has recently been identified as a significantly important factor complicating and impeding treatment response in a number of solid tumors. This heterogeneity giving rise to diverse phenotypes may be explained by both the standard theory of clonal evolution, and the cancer stem cell (CSC) hypothesis[11]. The theory of clonal evolution states that most tumors arise from single cells through the sequential accumulation of numerous genetic changes and epigenetic modifications. However, the cancer stem cell hypothesis suggests that only a sub-population of so-called "cancer initiating cells" have the

capacity for unlimited proliferation and are therefore responsible for the initiation and maintenance of tumors [12]–[14]. Purported cancer stem cells, in addition to their ability to self-renew indefinitely, may undergo symmetric or asymmetric "unidirectional" divisions along a hierarchy of differentiation to generate daughter cells with low tumorigenic potential (non-CSCs) [12], [15]. However, recent experimental studies have suggested that the unidirectional hierarchy model of CSCs should be modified to account for experimental evidence suggesting a degree of plasticity between the non-CSC and CSC compartments[9]. The dedifferentiation of non-CSCs into CSCs may also arise due to stochastically acquired genetic or epigenetic changes in genes governing the CSC state. For instance, recent studies have shown that overexpression of BMI1 (polycomb ring finger oncogene) in transformed epithelial cells can promote their conversion into a CSC-like state with increasing tumorigenicity and metastatic potential[11]. Interestingly, BMI1 has also recently been shown to be critical for stem cell self-renewal in brain tumors and is an indicator of poor prognosis [16]. The dedifferentiation of non-CSCs into CSCs may also be driven by the epithelial to mesenchymal transition (EMT), a cellular differentiation program wherein epithelial cells adopt mesenchymal features. Recent studies have also linked the EMT with the acquisition of stem-cell-like characteristics [17].

The main translational implications of the CSC model and tumor plasticity lie in the planning of appropriate and efficacious treatment strategies. Importantly, several studies have indicated that CSCs are resistant to many of the standard therapeutic regimes, including chemotherapy and radiation therapy [18], [19]. In fact, experimental studies have shown an increase in the expression of CSC markers and the self-renewal capacity after these treatments, suggesting the presence of a treatment-refractory CSC population. Moreover, therapies that target primarily CSCs may ultimately be unsuccessful if non-CSCs are able to dedifferentiate into a CSC state. If at least some differentiated cells possess the plasticity enabling them to revert to a stem-like state, then reconciliation with the cancer stem cell hypothesis results in a dynamic and robust pool of CSCs that is difficult to completely eradicate. Hence, it is of critical importance to develop a deeper understanding of the plasticity and heterogeneity of cancer cells to overcome these therapeutic limitations. We argue that appropriate mathematical models, based on

sufficient experimental data, can help in understanding the cancer stem cell hypothesis and characterizing the phenotypic plasticity of cells.

Several mathematical models have been developed to study the heterogeneity of cancer cells and the CSC hypothesis [20]–[26]. Recently, theoretical approaches have been also used to better understand and characterize the nature of tumor cell plasticity. Two classes of mathematical models have been developed – those that incorporate an essential hierarchy of differentiation, and those that do not, and can be thought of as phenomenological models. A biological justification for a hierarchical model of phenotypic plasticity is inspired by the process of differentiation that is known to occur within normal stem cell populations, whereby stem cells differentiate into progenitor cells which have a limited number of possible self-renewals and then finally into mature, fully differentiated cells. Turner and Kohandel generalized the hierarchical model of CSCs to include the dedifferentiation from non-CSCs to CSCs due to the EMT [27]. They utilized a stochastic model in the case of a small number of cells comprising a tumor (simulating the experimental tumorsphere formation assay), while a related deterministic model is used for larger cell populations. Chaffer et al. (2011) and Gupta et al. (2011) also developed non-hierarchical deterministic models to quantitatively describe phenotype switching between subpopulations of cancer cells [9], [10].

Gupta et al. (2011) suggested a model of one stem cell and two epithelial (basal and luminal) phenotypes for SUM159 and SUM149 breast cancer cell lines [9]. The CD44hi/CD24lo marker is considered the primary marker of stemness while EpCAM (or ESA) is used to distinguish basal cells from CSCs. In their model, all three phenotypes have proliferative capacity and a finite transition probability between all the three phenotypes is developed to explain the observed results. For the SUM149 cell line, it is observed that the dominant transition from the stem cell phenotype is switching into a luminal cell, whereas for a SUM159 cancer stem cell, the dominant transition is found to be into a basal cell type. The numerical values for stem cell and non-stem cell proliferation rates and the phenotype switching transition rates are obtained by matching the model results with observed steady state fractions of the three sub-populations (after 12 days). The growth rates are measured for either of the sub-populations (filtered by

FACS) confirming a proliferation potential of all sub-populations. However, their approach is based on a few main assumptions as described below.

First, in a non-hierarchical model of stem cell proliferation, the mathematical models formed often require self-renewal proliferation rates on non-stem cell populations, essentially conferring the unique stemness property on inherently non-stem cell populations. Thus, mathematically, such a model is sufficient to explain the phenotype switching phenomena up to fitting the parameters, but the underlying biology relies upon an assumption that may be inherently flawed. Hence, the dynamics of such models, apart from their steady states, should not be assumed to be experimentally valid. In fact, mathematical analyses have shown that the proliferation potential of non-CSCs may not reproduce biologic observations and that the generational hierarchy appears to play an important role in overall tumor growth [25].

A second issue arises with regards to the identification of CSCs. All currently available methods for isolating, or enriching for CSCs rely upon the use of a biomarker or a combination of biomarkers, such as CD133, GD2, or CD44/CD24. However, it has been shown that isolating based only on fluorescence levels of these biomarkers is insufficient to purify only CSCs, experimentally confirmed by the fact that when these biomarker positive cells are disaggregated into single cell suspensions, not all form tumorspheres, or aggregates of cells[28]. Thus, the employed biomarkers are imperfect and experimental data supports the hypothesis of the existence of a subpopulation of non-CSCs that are biomarker positive. To address this imperfectness, Zapperi and La Porta (2012) used a hierarchical model to describe the same results via direct inclusion of the effect of imperfectness in biomarkers [29]. The imperfectness is considered in following way: the biomarker-positive subpopulation is defined such that it may include a small population of non-CSCs, and the biomarker-negative subpopulation is defined such that it may include a small population of CSCs. For example, differentiated cells generally are biomarker-negative, but within this biomarker-negative group, some CSCs are accounted for, to correct for an imperfection in the biomarker identification of these CSCs. In each cell division, every positive (or negative) cell has the potential to divide into two positive daughter cells, or one positive and one negative cell with

different, but fixed, probabilities. Authors were able to fit the growth rate plot of Gupta et al. (2011) using this hierarchical model [9]. Turner and Kohandel (2010) used an alternative method to incorporate the biomarker imperfectness, supposing that as cells differentiate, they become increasingly committed, and therefore downregulate the expression of proteins that would make them stem-like [27]. Thus, they assumed that the biomarker is retained for CSCs and the first few generations of progenitor cells, to account for its imperfectness, and then after those biomarker positive generations of progenitor cells, the remaining cells of the hierarchy are biomarker negative.

A main shortcoming in some of the previous studies, namely Chaffer et al. (2011), Gupta et al. (2011), Zapperi and La Porta (2012), is that these studies are fully based on deterministic approaches to validate the corresponding experimental data with large numbers of cells including fraction of CSCs and population doublings (PD). Although their models agree well with the corresponding experimental data, lack of data from mammosphere formation assays conceals the stochastic behavior of cancer cells, which becomes relevant when small numbers of cells are considered.

In this work, we show that stochastic effects play a critical role in tumor cell behavior, and that model validation using experimental data quantifying these stochastic effects, such as sphere-formation assays, is critical [30]. To this end, we develop a stochastic model describing a two-compartment phenotype switching model, as originally suggested in Gupta et al. (2011), and compare model simulation results with a hierarchical model of CSC proliferation, adapted from the work of Turner and Kohandel (2012). We show that the two models give the same deterministic behavior, but give significantly different stochastic behavior. This not only supports the application of both deterministic and stochastic approaches to study cancer heterogeneity and plasticity, but also it stresses the importance of sphere formation assays to obtain a more accurate description of the system being studied.

2.2 Method

We consider two mathematical models: a two-compartment model (TCM), as used by Chaffer et al. (2011) and Gupta et al. (2011), depicted in Fig.4(a), and a hierarchy model (HM), adapted from the work of Turner and Kohandel (2012), shown in Fig. 4(b). We investigate the behavior of the population of cancer cells for both small and large numbers of cells to compare their stochastic and deterministic properties.

The two-compartment model consists of two phenotypically distinct cellular subpopulations of biomarker negative and positive cells, for instance CD44highCD24low and CD44lowCD24high in breast cancer, each with the ability to self-replicate and the ability to transition into the other phenotype. We also add cell death as one of the possible changes in each subpopulation, as depicted in Fig. 4(a). Adding a distinct death rate is required to accurately model the experimental behavior of the cancer cells in small populations such as the growth of the cells in the MFA. We show that the birth and death rate can be combined into a proliferation rate without any change in the deterministic properties of the system, but a combined net proliferation rate is not a sufficient system descriptor when stochastic effects are taken into consideration, in theory. The models also take into account dedifferentiation, or the conversion of non-CSCs into CSCs, by accounting for this reverse reaction. Additionally, to model the concept that the biomarker used to distinguish the CSCs is imperfect, following Turner and Kohandel (2012), we suppose that the first k generations of progenitor cells are biomarker positive (Fig. 4(b)).

Here we present the details of the two-compartment model (TCM) and the hierarchical model (HM) as discussed in the main text. The deterministic behavior of each sub-population is modeled using ordinary differential equations and the stochastic behavior modeled is described by master equations.

2.2.1 Two compartment model

The following system of ordinary differential equations defines the deterministic behavior of both CSCs (*S*), assumed to be positive biomarker, and non-CSCs (*P*), assumed to be biomarker negative, in the TCM:

$$\begin{aligned}\frac{dS}{dt} &= (\rho_{ss} - \rho_{sp})S + \rho_{ps}P \\ \frac{dP}{dt} &= (\rho_{pp} - \rho_{ps})P + \rho_{sp}S\end{aligned} \tag{2.1}$$

Here ρ_{ss} and ρ_{pp} are self-renewal rates of CSCs and non-CSCs, respectively. The coefficients ρ_{sp} and ρ_{ps} represent the switching rates between the two compartments. In order to obtain the fraction of each sub-population, we define:

$$F_{\text{positive}}(t) = \frac{S(t)}{S(t)+P(t)}, F_{\text{negative}}(t) = \frac{P(t)}{S(t)+P(t)} \tag{2.2}$$

In the steady state, we have:

$$\begin{aligned}F_{\text{positive}} = \frac{\gamma_1 + \sqrt{\gamma_1^2 - 4\gamma_2}}{2},\ F_{\text{negative}} = 1 - F_{\text{positive}},\quad \gamma_1 \\ = \frac{\rho_{pp} + \rho_{ps} + \rho_{sp} - \rho_{ss}}{\rho_{pp} - \rho_{ss}},\quad \gamma_2 = \frac{\rho_{ps}}{\rho_{pp} - \rho_{ss}}\end{aligned} \tag{2.3}$$

In order to investigate the stochastic behavior of the cancer cells in the TCM, we write the corresponding master equation for the joint probability function:

$$\begin{aligned}\frac{\partial p(n_S, n_P, t)}{\partial t} &= \rho_{SS}(n_S - 1)p(n_S - 1, n_P, t) + \rho_{PP}(n_P - 1)p(n_S, n_P - 1, t) \\ &+ \rho_{SP}(n_S + 1)p(n_S + 1, n_P - 1, t) + \rho_{PS}(n_P + 1)p(n_S - 1, n_P + 1, t) \\ &+ \Gamma_S(n_S + 1)p(n_S + 1, n_P, t) + \Gamma_P(n_P + 1)p(n_S, n_P + 1, t) \\ &- [(\rho_{SS} + \rho_{SP} + \Gamma_S)n_S + (\rho_{PP} + \rho_{PS} + \Gamma_P)n_P]p(n_S, n_P, t)\end{aligned} \tag{2.4}$$

where we have assumed that at the initial time t_0, the number of each type of cell is known and these values are denoted n_S^0 and n_P^0 for CSCs and non-CSCs, respectively.

2.2.2 Hierarchy model

The following ordinary differential equations present the deterministic behavior for each sub-population of cells in the hierarchy model, based on the divisions and switching shown in Fig. 4:

$$\begin{aligned}
\frac{dS}{dt} &= \rho_S(r_1 - r_3)S + \gamma_p P_1 \\
\frac{dP_1}{dt} &= -(\gamma_p + \Gamma_p + \rho_p)P_1 + \rho_S(r_2 + 2r_3)S + \gamma_p P_2 \\
\frac{dP_i}{dt} &= -(\gamma_p + \Gamma_p + \rho_p)P_i + 2\rho_P P_{i-1} + \gamma_p P_{i+1},\ i = [2, \dots, k-1] \\
\frac{dP_m}{dt} &= -(\gamma_p + \Gamma_p)P_m + 2\rho_P P_{m-1}
\end{aligned} \tag{2.5}$$

Similar to the TCM, we may define a function representing the fraction of positive and negative cells. We assume that the stem and the first k generations of progenitor cells are biomarker positive cells. The steady state values for these functions are then solved for numerically.

The stochastic behavior for the cancer cell population can also be obtained using the master equation as follows:

$$\frac{\partial p\left(n_S, n_{P_1}, \dots, n_{P_m}, t\right)}{\partial t}$$

$$\begin{aligned}
&= \rho_S r_1 (n_S - 1) p\left(n_S - 1, n_{P_1}, \dots, n_{P_m}, t\right) \\
&+ \rho_S r_2 n_S p\left(n_S, n_{P_1} - 1, \dots, n_{P_m}, t\right) \\
&+ \rho_S r_3 (n_S + 1) p\left(n_S + 1, n_{P_1} - 2, \dots, n_{P_m}, t\right) \\
&+ \gamma_p \left(n_{P_1} + 1\right) p\left(n_S - 1, n_{P_1} + 1, \dots, n_{P_m}, t\right) \\
&+ \sum_{i=2}^{m} \rho_P \left(n_{P_{i-1}} + 1\right) p\left(n_S, n_{P_1}, \dots n_{P_{i-1}} + 1, n_{P_i} - 2, \dots, n_{P_m}, t\right) \\
&+ \sum_{i=2}^{m} \gamma_p \left(n_{P_i} + 1\right) p\left(n_S, n_{P_1}, \dots n_{P_{i-1}} - 1, n_{P_i} + 1, \dots, n_{P_m}, t\right) \\
&+ \Gamma_S (n_S + 1) p\left(n_S + 1, n_{P_1}, \dots, n_{P_m}, t\right) \\
&+ \sum_{i=2}^{m} \Gamma_P \left(n_{P_i} + 1\right) p\left(n_S, n_{P_1}, \dots n_{P_i} + 1, \dots, n_{P_m}, t\right) \\
&- \left[(\rho_S + \Gamma_S) n_S + \sum_{i=1}^{m} \left(\rho_P + \Gamma_P + \gamma_p\right) n_{P_i} \right] p\left(n_S, n_{P_1}, \dots, n_{P_m}, t\right)
\end{aligned} \tag{2.6}$$

where the parameters are defined in the reactions presented in Fig.4(b).

The corresponding equations are either solved analytically or numerically, and stochastic simulations are performed employing the well-known Gillespie algorithm [31]. In this approach, a random number is generated, and used to determine when the next cell division will occur, and what type of division it will be. The time evolution is then simulated over an appropriate number of days of a colony of cells originating from one or more cancer cells at the initial time. This procedure can be practically described through the following five steps:

1. Set the initial state $n = n_0$ at $t = t_0$ (the state n of the Markov process is a vector quantity).
2. Consider the waiting time τ until the next transition occurs. This could be obtained as follows

   $$\tau = (1/a(n)) ln\, 1/\sigma_1$$

   where σ_1 is a random number and $a(n)$ is defined as

   $$a(n) = \sum_{i=1}^{M} c_i n_i$$

where the index i runs over all possible divisions and switching pathways of the process. In addition, c_i is the probability per unit time that an individual cell will undergo division i and n_i is the number of cells that may undergo division i. In the procedure of the Gillespie algorithm, we use division as both division and switching for simplification.

3. Choose k so that the system goes to state n^* at time $t + \tau$. By choosing a random number σ_2, the division is chosen to satisfy the following relation

$$\sum_{i=1}^{k-1} a_i < \sigma_2 a(n) < \sum_{i=1}^{k} a_i$$

4. Update the system according to $t = t + \tau$, $n = n_k$.
5. Return to step 2.

In order to numerically solve the equations representing the TCM and HM for the data presented in Gupta et al. (2011), suitable parameters had to be obtained. However, first we note that the data in Gupta et al. (2011) is presented for three distinct cellular subpopulations comprising the tumor, but within TCM we consider only two. That is, in order to fit the data presented by Gupta et al. (2011), we simplify their results to include only CSCs and non-CSCs, by summing the experimental data points for the non-stem populations studied, in the same method as presented by Zapperi and La Porta (2012). Furthermore, in order to extract parameters to model the system given the experimental results of Gupta et al. (2011), a brute force parameter search was carried out. The parameter space was sampled discretely, and over the space, combinations of parameter sets, chosen between 0 and 1, were simulated with the deterministic equations, deriving a steady state value for the system. If this steady state value was within a small tolerance of that observed by Gupta et al. (2011), then the parameters used were taken as a viable parameter set. The criteria for obtaining a suitable parameter set was such that the parameters must have satisfied the steady state within a small tolerance value, and reach it by a specified cutoff time for the cases of initial conditions of only biomarker positive cells, only biomarker negative cells, and a random number of biomarker positive cells, binomially distributed about a known mean value. Additional experimental results that were used to obtain parameter sets (Table 7 and 8) were the fraction of CSCs after 6 days of culture (Table 6) and PD at $t = 1$ and $t = 2$ (Gupta et al. (2011)).

Table 6 Cellular subpopulations in stem-like (SL), and non stem-like (average of basal and luminal states) were isolated by FACS with antibodies directed against the CD44, CD24, and EpCAM cell surface antigens. The values show the fraction of cells in each cell-differentiation state as assessed by FACS after in vitro culture for 6 days. (Gupta et al (2011),).

Subpopulations	Fraction of CSCs	Fraction of luminal plus basal cells
SL cells	3.8	96.2
Average of luminal and basal cells	2.2	97.8

Table 7 Parameter values and their standard deviations for the TCM, obtained by fitting to the data available in Gupta et al (2011) (Unit of all numbers is $(1/day)$).

Rates	ρ_{SS}	ρ_{PP}	ρ_{PS}	ρ_{SP}
Average	0.76	0.6412	0.0168	0.8335
Standard deviation	0	0.0264	0.0013	0.0023

Table 8 Parameter values and their standard deviation for the HM, obtained by fitting to the data available in Gupta et al (2011) (Unit of all numbers is $(1/day)$).

Parameters	$\rho_S r_1$	$\rho_S r_2$	$\rho_S r_3$	ρ_P	γ_P
$N = 5$	0.01(0)	0.43(0.012)	0.07(0.001)	1.72(0.054)	0.64(0.017)
$N = 12$	0.01(0)	0.05(0.002)	0.64(0.021)	0.93(0.021)	1.01(0.032)

We use the obtained parameter sets to show the accuracy of our analysis (Figs. 5 and 6). It is clear that at the considered points, the time stages we have experimental data, our results are in good agreement with the experiments. The deterministic results of both TCM and HM used

to verify the modeling are almost the same after day 5 at which we have the experimental data (Figs. 5 and 6).

2.3 Results

2.3.1 Two compartment model

We begin by fitting parameters using the described parameter search to the TCM for the experimental results of Gupta et al. (2011). The simulated data using the obtained parameters give us quantitative results that are in strong agreement with the experimental data, suggesting a well-fitting model. We observe in Table 7 that the parameter values obtained are scattered around average values, with a small standard deviation, suggesting that they are associated in the parameter space. Moreover, we point out that these parameter sets are not unique, and although the deterministic behavior for each of these parameter sets is the same by their definition, we must also analyze how their differences affect the stochastic behavior of the population. Specifically, we analyze the stochastic behavior of the system, considering the MFA. The start of the MFA typically involves 1000 or more wells with few cells in each well and the cells grow for a small number of days, and the MFA is given as the proportion of wells with spheres of cells above a certain cutoff size. We simulate this experiment theoretically using TCM for two parameter sets in agreement with

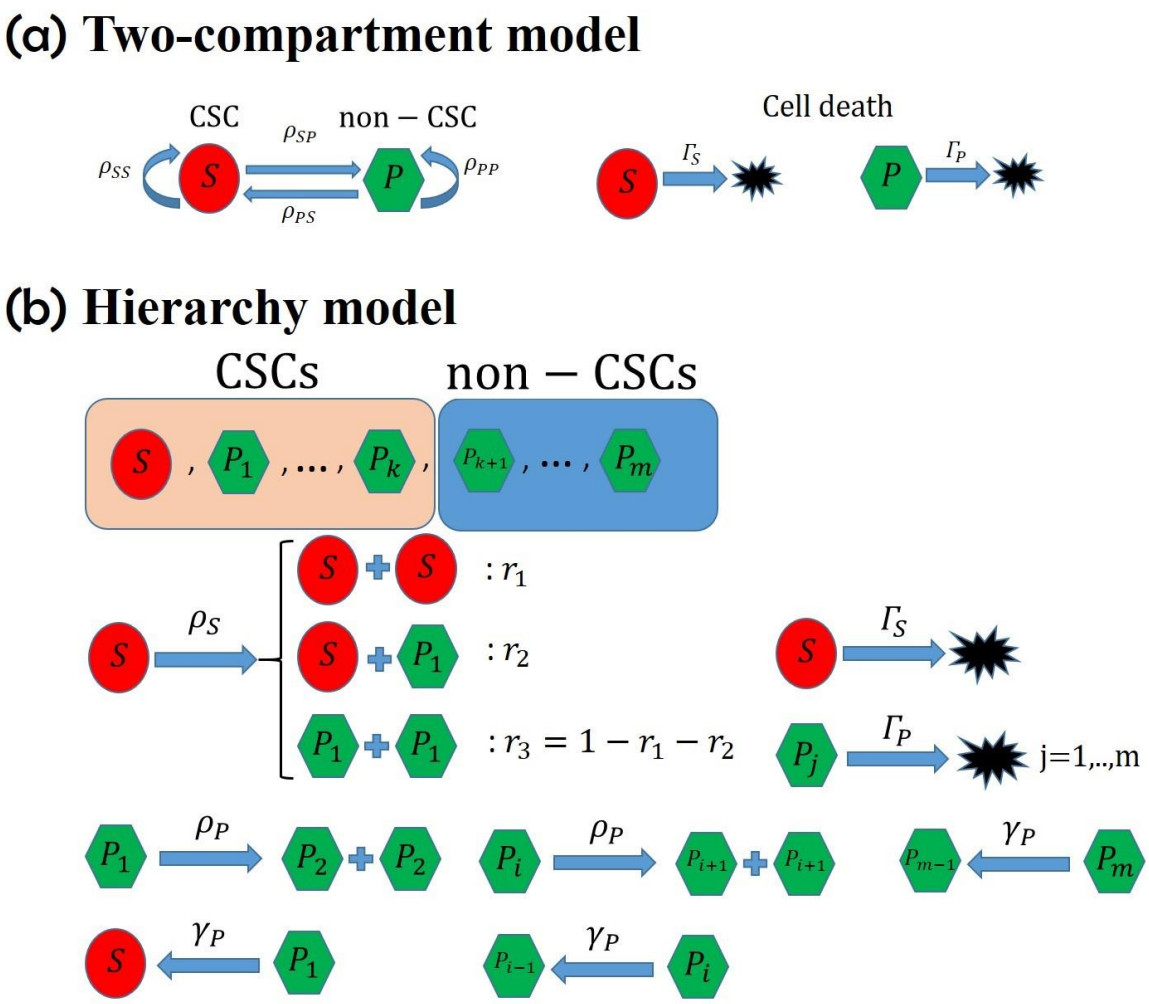

Figure 4 Schematic representation of (a) Two-compartment model (TCM) and (b) Hierarchy model (HM), where $i = 1, 2, \dots, k$.

the deterministic investigation by Gupta et al. (2011). Importantly, examining the number of mammospheres with respect to time, for each parameter set, as shown in Fig. 7, shows significant differences in the stochastic behavior of the two cases. In essence, this highlights the fact that the stochastic and deterministic properties of a system are quite different, and using experimentally observed deterministic criteria does not necessarily produce consistent stochastic behavior. Thus, in order to more exactly determine parametric descriptions of

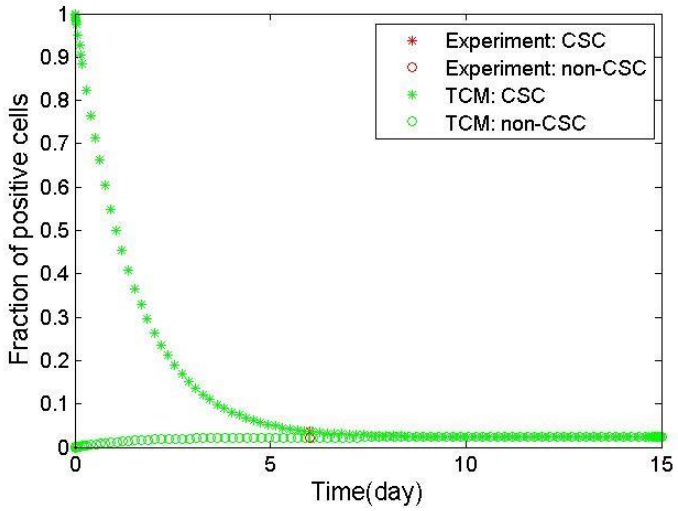

Figure 5 Time variation of fraction of positive cells based on the TCM.

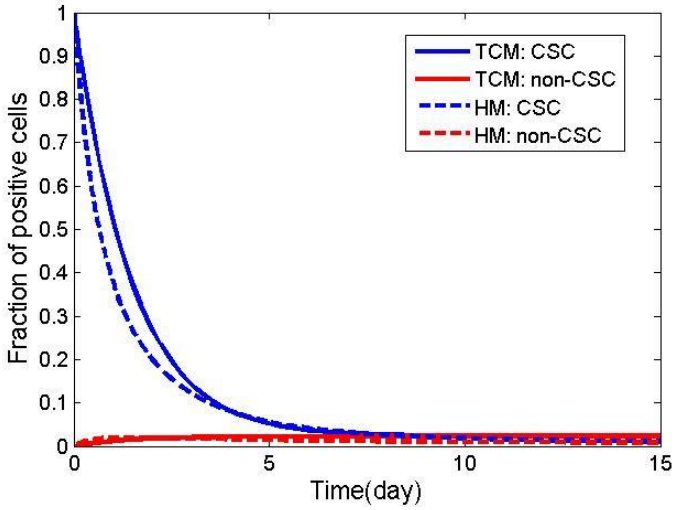

Figure 6 Fraction of positive cells as a function of time in the TCM and the HM (with 12 progenitor cells in the hierarchy).

experimental systems, both stochastic and deterministic studies must be carried out, or else vital characteristic information is lost.

The results in Fig. 7 also reveal an important artifact of the mathematical analysis, and a shortcoming of the model used that may not be necessarily biologically descriptive. That is, as

shown in Fig. 7, after a certain time point, for both parameter sets considered, every well contains an observable mammosphere, which almost certainly is not observed experimentally. We rectify this issue by the addition of a distinct death rate term in the mathematical modeling, which causes the demise of initiating cell populations before they are ever able to form mammospheres, resulting in more realistic simulated data.

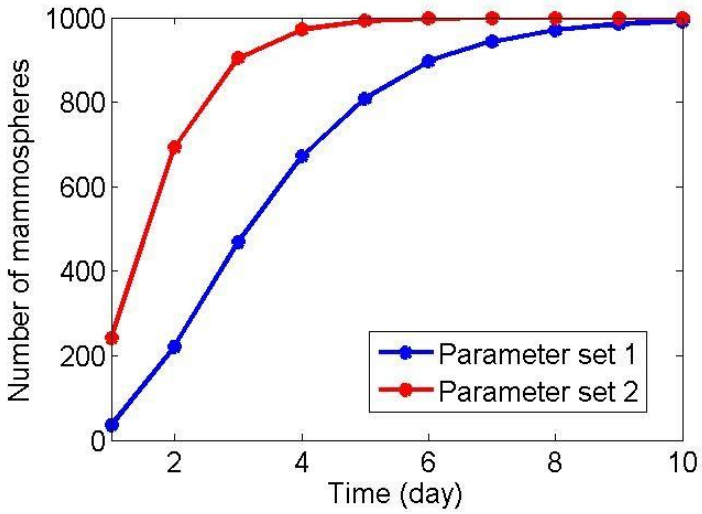

Figure 7 Variation of MFE with respect to time for two parameters sets: parameter set 1: $\rho_{SS} = 0.165, \rho_{SP} = 0.5050, \rho_{PS} = 0.015, \rho_{SS} = 0.385$; parameter set 2: $\rho_{SS} = 0.76, \rho_{SP} = 0.5050, \rho_{PS} = 0.015, \rho_{SS} = 0.945$. (All death rates are considered to be zero.)

Additionally, we now characterize the consequences for the stochastic behavior of the cancer cell population that a distinct cellular death rate parameter has. We do this by simulating the MFA, and results are illustrated in Fig. 8 using the model with varying death rates. These results show the effects of neglecting the death rate in the system, and we observe that in the case of no distinct cell death parameter, the mammosphere formation efficiency (MFE) approaches 100%, or that all cell colonies form mammospheres, which is an experimentally non-viable result, as previously discussed. Thus, in order to obtain a reasonable MFE, we argue that considering a separate cellular death rate parameter is a reasonable model consideration.

The effects of varying the death rate on average mammosphere size (AMS) as an experimentally measurable parameter are also significant (Fig. 9). It is shown that by increasing the death rate, the AMS increases. This may be explained in the sense that increasing the death rate results in fewer mammospheres developed, but of those that do develop, they develop faster and proliferate to a greater degree, because they must proliferate enough to reach the mammosphere cutoff size, in the presence of a death rate acting to reduce mammosphere size. In essence, this implies that the initial survival probability of the cells (or MFE) is related inversely to the AMS.

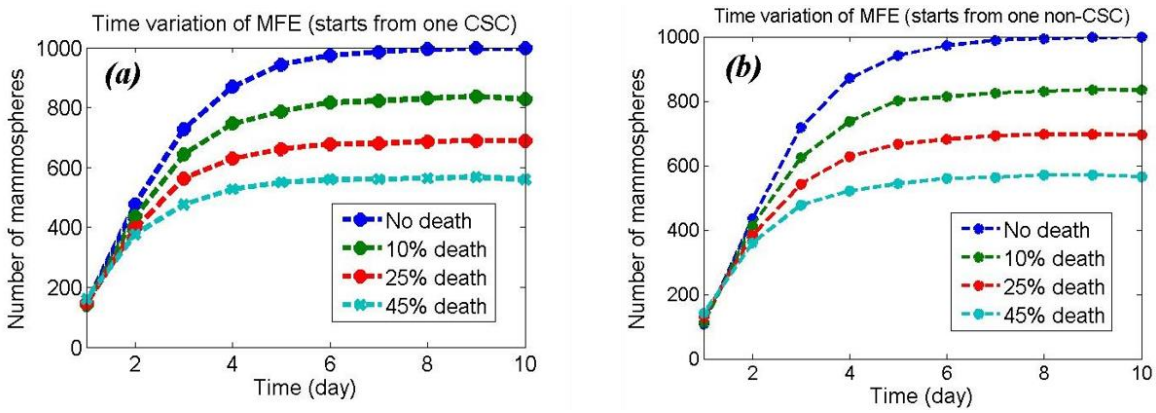

Figure 8 MFE of a simulated experiment using TCM started from (a) CSCs and (b) non-CSCs for different death rates. 1,000 single cells are considered initially in the simulated experiment.

In addition to death rate, the initial cellular composition of the mammosphere seeding population is an important determinant of the AMS. Although the effect of the initial cellular population composition on MFE is negligible (Fig. 8), there is a significant effect of the initial cellular population on the AMS (Fig. 9). That is, the AMS in cultures with an initial population comprised of CSCs is larger than the AMS for cultures with an initial population comprised of non-CSCs, as CSCs have a higher proliferative capacity than non-CSCs. The effect of death rate on the stochastic behavior of the cells can be also examined considering the survival probability of CSCs.

Plasticity is another key factor affecting the survival probability of CSCs, and we note that in the modeled system this is represented by the dedifferentiation of non-CSCs into CSCs, which results in the repopulation of the system, even when there are initially no CSCs. In order to study the effects of death rates on the survival probability of cancer cells, contours of survival probability are obtained, for varying degrees of plasticity and death rate (Fig. 10). Specifically, the CSC death rate is fixed, and the effects of varying the non-CSC death rate and ratio of dedifferentiation to differentiation, $R = \rho_{PS}/\rho_{SP}$ (a measure of plasticity) on the survival probability are illustrated. In the case of no CSC death rate (Fig. 10(a)), the survival probability increases as *R* increases, and for higher non-CSC death rates, this effect is more pronounced. It is shown that for low death rates of non-CSCs, the contour is stable, and it can be inferred that the survival probability is therefore relatively independent of the effects of dedifferentiation, or cellular plasticity.

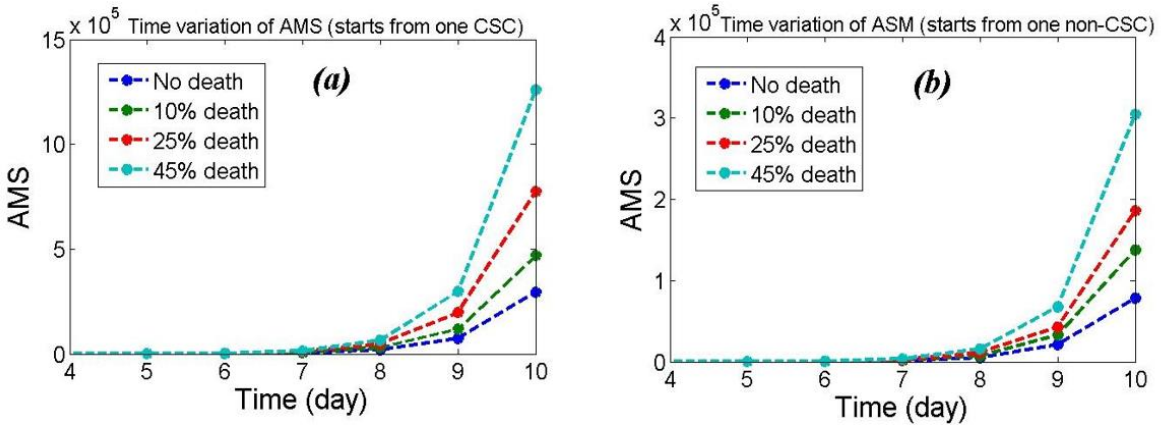

Figure 9 AMS of a simulated experiment using TCM started from (a) CSCs and (b) non-CSCs for different cell death rates. 1,000 wells, each with a single cell, are considered initially in the simulated experiment.

Increasing the CSC death rate to a nonzero value (*0.4*) reveals that in a region of high non-CSC death rate, as depicted in Fig. 10(b), the survival probability of CSCs is increased for higher values of *R*. The biological implication of this result is that increasing dedifferentiation results in a higher survival probability of CSCs. The shape of the contour for low non-CSC death rates is similar to the behavior of the contour for a zero CSC death rate, in that beneath

a certain threshold value, the survival probability of the CSCs decreases as the plasticity increases. This means that because of a nonzero CSC death rate, there is a threshold value of non-CSC death rate under which it is more advantageous for the survival of the CSCs to have a lower rate of dedifferentiation. Moreover, for a death rate of non-CSCs above this threshold, we see the reverse effect in which it becomes advantageous for a greater degree of dedifferentiation to occur. Interestingly, this analysis suggests that controlling either the death rates of CSCs and non-CSCs in certain regimes of plasticity results in non-intuitive behavior, which may be exploited clinically to reduce the MFE.

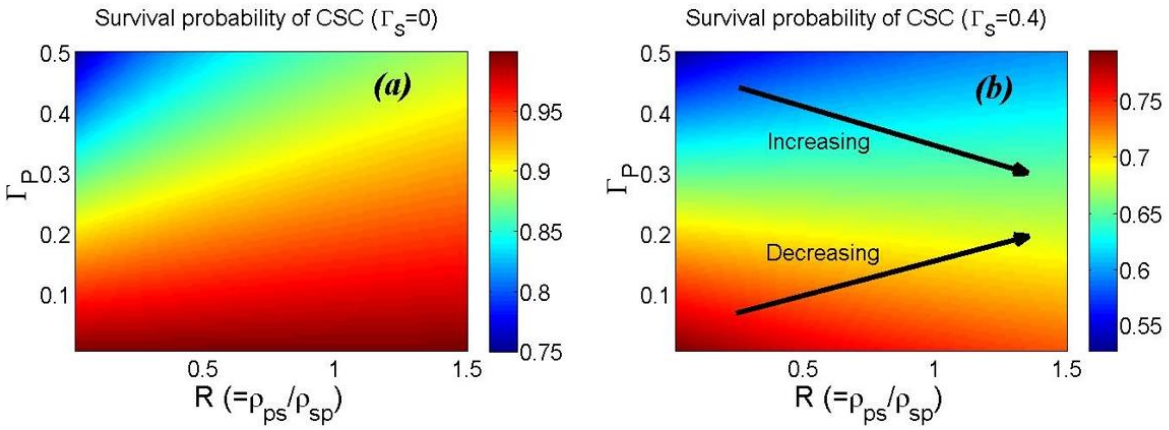

Figure 10 Survival probability contours of the CSCs as functions of non-CSC death rate and $R = \rho_{ps}/\rho_{sp}$ for CSC death rate to be equal to 0 (a) and 0.4 (b). The other parameters of the model are same as those in Table 7.

2.3.2 Hierarchy model

The parameters of the hierarchy model, as considered in this work, are derived in a manner similar to that of the TCM, and defined to approximate the experimental results of Gupta et al. (2011). Averages and standard deviations of the obtained parameter sets are presented in Table 8. The importance of stochastic analysis in defining accurate parameters is highlighted in the previous section using TCM and to avoid repetition, we proceed by directly analyzing the effect of death rate on the behavior of the cancer cell population. The mammosphere formation assay is simulated, and we observe that the HM is highly sensitive to the parameter representing cellular death rate, as depicted in Fig. 11(a). In this case, the MFE is changed by over 400 out

of 1,000 cultures by increasing the death rate only by 12%. To obtain a similar effect for TCM, the death rate would have to be increased by more than 30%, and thus it is less sensitive to the cellular death rate. Additionally, in HM, as was seen for TCM, the initial cell composition in the mammosphere formation assay impacts the behavior of the cancer cell population (Fig. 11(b)). Specifically, starting from further differentiated cells, or later cell generations, results in fewer formed mammospheres, as may be expected since these cells have a reduced proliferative capacity, compared to those cells earlier in the hierarchy. Interestingly, we note that the dependency of MFE on the initial cell hierarchy level (ICL) is nonlinear and changing the ICL significantly changes MFE. In describing this nonlinearity, it appears thatthe MFE is relatively insensitive to ICLs at medial levels, but more sensitive to ICLs closer to the upper and lower bounds of the generational levels within the hierarchy model.

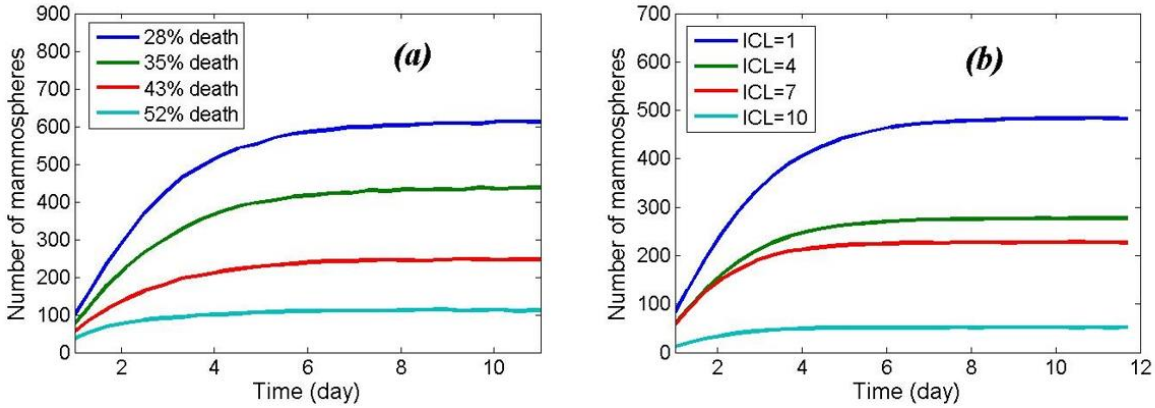

Figure 11 MFE of a simulated experiment using HM for different (a) death rates (start with CSC) and (b) initial cell level (ICL) (death rate=25%). 1,000 cells are considered initially in the simulated experiment.

Within the HM, we suppose that the death rates of CSC and all generations of non-CSCs are equal. It is observed that in the case of lower death rates, the number of cells increases very quickly, resulting in a higher MFE. Lastly, we notice that for HM, as is the case with TCM, the MFE is 100% in the case of a zero death rate, suggesting that every culture would produce mammospheres, even though experimentally this is unviable, and underscores again the importance of including a distinct cellular death parameter, when describing experimental data.

In examining the time variation of the AMS for the HM, as death rate is varied, as is depicted in Fig. 12(a), we observe that the saturation for the AMS is highly sensitive to the death rate. That is, for lower death rates, much higher AMS values are observed at saturation. We also examine the dependency of AMS on ICL, as shown in Fig. 12(b). From this graph, it may be observed that the saturation of the AMS is dependent on the ICL in a significant manner. For lower ICL, the cellular proliferative capacities are higher, and thus, as expected, form larger mammospheres on average. We note that this analysis of the AMS shows that it is sensitive in saturation to parameters such as the cellular death rate, and the ICL, and because it is experimentally observable, may provide a useful adjunct when validating experimental data against mathematical models, to better characterize the behavior of such cell populations.

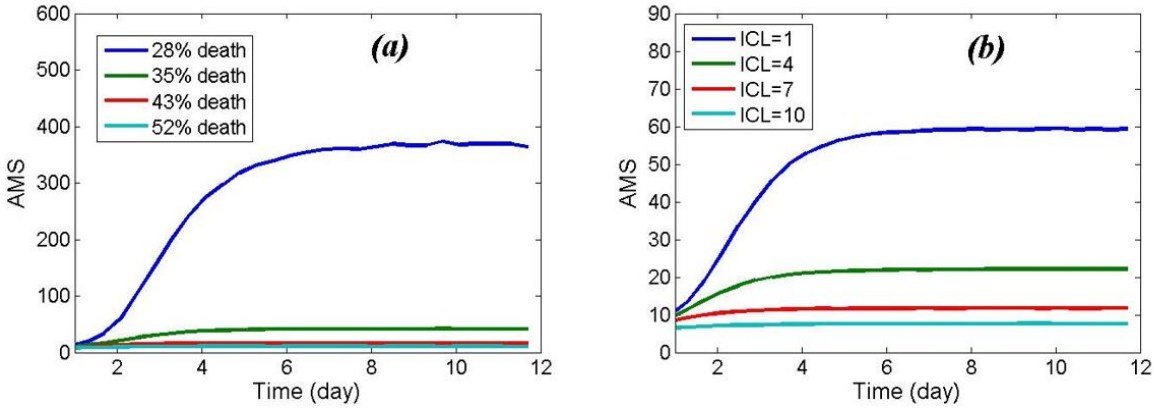

Figure 12 AMS of a simulated experiment using HM for different (a) death rates (start with CSC) and (b) initial cell level (ICL) (death rate=25%).

The observed sensitivity of experimentally observable model outputs, such as the MFE or AMS to the ICL highlights the importance of considering biomarker imperfectness as explicative of obtained results. Biomarker imperfectness would result in an ICL that may be higher or lower than expected, depending on the unobservable true cellular composition, and therefore could potentially significantly affect the observed MFE and AMS.

We now compare the TCM and HM in the limit of large cellular populations, in contrast to the stochastic behavior analysis presented above. In the large number limit for cell population, we show that the dynamics for the system described by HM converges to that of TCM. In order to

examine this closely, we use the time variation of the number of population doublings. This quantity can be defined mathematically as:

$$\mathrm{PD} = \log(\text{cell number}/\text{initial cell number}) \,/\, \log 2$$

We now analyze HM and its fit to the corresponding population doublings curve as determined by the results of Gupta et al. (2011). The population doublings diagram depicted in Fig. 13(a) is a theoretical result for 5 generations of progenitor cells in HM, whereas the diagram in Fig. 13(b) is a theoretical population doublings curve for 12 generations of progenitor cells in HM. We observe that the degree of fit to experimental data is stronger when HM is considered to be comprised of 12 generations of progenitor cells. In addition, we observe in Fig. 13 that modeling the time evolution of the population doublings curve for the HM converges to the analogous behavior of the TCM in the limit of large cell numbers, implying that deterministically, the solutions to each model are the same.

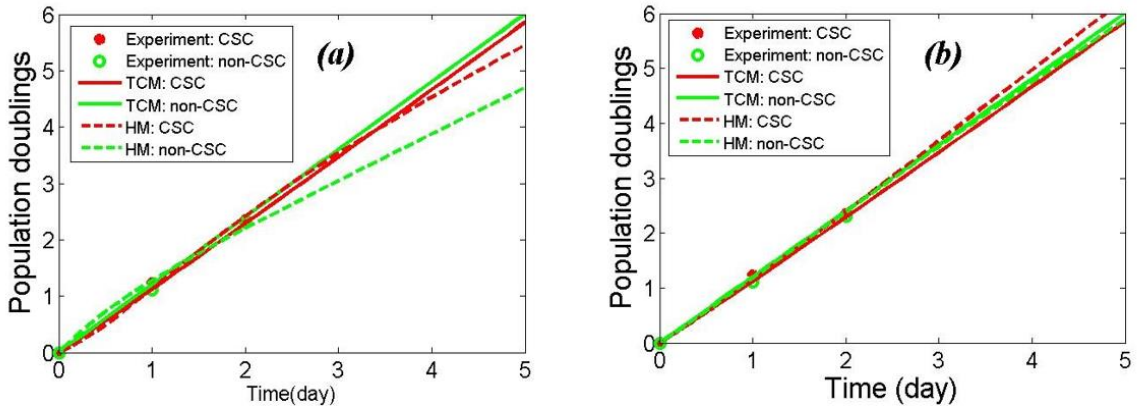

Figure 13 Comparison of population doublings from experiment Gupta et al. (2011) and by hierarchy model with (a) 5 and (b) 12 progenitor levels in the hierarchy.

2.4 Sensitivity analysis

In this section, we want to obtain the analytical solution of the deterministic equations of TCM (Eq. (2.1)) and use to investigate the sensitivity of the model to the rate of plasticity. This analysis help us to understand the effect of plasticity on the model results for different ranges of the other model parameters.

To simplify our analysis we rename the positive fraction to X instead of $F_{positive}$. Therefore, the definition of this parameter, as a function of S and P, will be

$$X = \frac{S}{S+P} \tag{2.7}$$

in which $S = S(t)$ and $P = P(t)$. We want to obtain X as a function of time and independent of the variables S and P. Taking derivative of Eq. (2.7) results in

$$\dot{X} = \frac{\dot{S}(S+P) - (\dot{S}+\dot{P})S}{(S+P)^2} \Rightarrow \dot{X} = \frac{\dot{S}}{(S+P)} - \frac{(\dot{S}+\dot{P})}{(S+P)}X \tag{2.8}$$

Substituting the time derivatives of S and P from Eq. (2.1) gives us the following equation.

$$\begin{aligned} \dot{X} &= \frac{(\rho_{ss}-\rho_{sp})S + \rho_{ps}P}{(S+P)} - \left(\rho_{ss}\frac{S}{(S+P)} + \rho_{pp}\frac{P}{(S+P)}\right)X \\ \Rightarrow \dot{X} &= (\rho_{ss}-\rho_{sp})X + \rho_{ps}(1-X) - \left(\rho_{ss}X + \rho_{pp}(1-X)\right)X \\ \Rightarrow \dot{X} &= -(\rho_{ss}-\rho_{pp})X^2 + \left((\rho_{ss}-\rho_{pp}) - (\rho_{sp}+\rho_{ps})\right)X + \rho_{ps} \end{aligned} \tag{2.9}$$

Considering three new parameters $a = \rho_{ss} - \rho_{pp}$, $c = \rho_{ps}$, and $b = a - c - \rho_{sp}$, we can rewrite the above equation as follows

$$\begin{aligned} \dot{X} &= -aX^2 + bX + c \\ \Rightarrow \dot{X} &= -a\left(X - \frac{b}{2a}\right)^2 + \left(c + \frac{b^2}{4a}\right) \\ \Rightarrow \dot{X} &= -a(X-\kappa)^2 + \gamma \end{aligned} \tag{2.10}$$

where $\kappa = b/2a$ and $\gamma = c + b^2/4a$. By considering the change of variable $y = X - \kappa$, we can obtain the following equation using Eq. (2.10)

$$\dot{y} = -ay^2 + \gamma \tag{2.11}$$

which can be changed to the following integral equation

$$\int \frac{dy}{\gamma - ay^2} = \int dt \tag{2.12}$$

Taking definite integral from both sides of this equation (from initial condition to the present state), using a new change of variable$\sqrt{a/\gamma}y = \sin(z)$, results in the following solution

$$\frac{1}{\sqrt{a\gamma}}\ln\left(\frac{\sec(z)+\tan(z)}{\sec(z_0)+\tan(z_0)}\right)=t$$

$$\Rightarrow \frac{1}{\sqrt{a\gamma}}\ln\left(\frac{\dfrac{1+\sqrt{\frac{a}{\gamma}}\mathrm{y}}{\sqrt{1-\left(\frac{a}{\gamma}\right)y^2}}}{\dfrac{1+\sqrt{\frac{a}{\gamma}}\mathrm{y}_0}{\sqrt{1-\left(\frac{a}{\gamma}\right)y_0^2}}}\right)=t \qquad \textbf{(2.13)}$$

$$\Rightarrow \frac{1+\sqrt{\frac{a}{\gamma}}\mathrm{y}}{\sqrt{1-\left(\frac{a}{\gamma}\right)y^2}}=\frac{1+\sqrt{\frac{a}{\gamma}}\mathrm{y}_0}{\sqrt{1-\left(\frac{a}{\gamma}\right)y_0^2}}\exp\left(\sqrt{a\gamma}t\right)$$

$$\Rightarrow \frac{1+\sqrt{\frac{a}{\gamma}}\mathrm{y}}{1-\sqrt{\frac{a}{\gamma}}\mathrm{y}}=\frac{1+\sqrt{\frac{a}{\gamma}}\mathrm{y}_0}{1-\sqrt{\frac{a}{\gamma}}\mathrm{y}_0}\exp\left(2\sqrt{a\gamma}t\right)$$

If we consider the right hand side of the last equation in Eq. (2.13) to be *B*, we can obtain *y* as a function of *B* as follows

$$y=\sqrt{\frac{\gamma}{a}}\frac{B-1}{B+1}$$

$$\Rightarrow X-\kappa=\sqrt{\frac{\gamma}{a}}\frac{B-1}{B+1} \qquad \textbf{(2.14)}$$

$$\Rightarrow X=\kappa+\sqrt{\frac{\gamma}{a}}\frac{B-1}{B+1}$$

Which can be rewritten as

$$X=\beta_1+\beta_2\frac{\exp(\alpha t)-\lambda/A}{\exp(\alpha t)+\lambda/A} \qquad \textbf{(2.15)}$$

where $\beta_1=\kappa$, $\beta_2=\sqrt{\frac{\gamma}{a}}$, $\alpha=2\sqrt{a\gamma}$, $\lambda=1-\sqrt{\frac{a}{\gamma}}y_0$, and $A=1+\sqrt{\frac{a}{\gamma}}y_0$. We can also obtain the first and second derivative of *X* as follows

$$\dot{X} = \beta_2 \frac{\alpha \exp(\alpha t)\left(\exp(\alpha t) + \frac{\lambda}{A}\right) - \alpha \exp(\alpha t)\left(\exp(\alpha t) - \frac{\lambda}{A}\right)}{\left(\exp(\alpha t) + \frac{\lambda}{A}\right)^2}$$

$$\Rightarrow \dot{X} = \beta_2 \frac{\frac{2\alpha\lambda}{A}\exp(\alpha t)}{\left(\exp(\alpha t) + \frac{\lambda}{A}\right)^2} \quad \textbf{(2.16)}$$

and

$$\ddot{X} = \frac{2\alpha\beta_2\lambda}{A} \frac{\alpha \exp(\alpha t)\left(\exp(\alpha t) + \frac{\lambda}{A}\right) - 2\alpha \exp(2\alpha t)}{\left(\exp(\alpha t) + \frac{\lambda}{A}\right)^3}$$

$$\Rightarrow \ddot{X} = \frac{2\alpha^2\beta_2\lambda}{A} \frac{\exp(\alpha t)\left(\frac{\lambda}{A} - \exp(\alpha t)\right)}{\left(\exp(\alpha t) + \frac{\lambda}{A}\right)^3} \quad \textbf{(2.17)}$$

We used the attained analytical solution of *X* and its time derivative and show the dependency of the time variation of the solution on the plasticity (Fig. 14). Changing the plasticity clearly change the time variation of *X* as illustrated in Fig. 14. In Fig. 14(a) and (c), it is shown that the higher plasticity makes the system toward faster equilibrium and change the curvature of the diagram. To clarify this dependency, $\dot{X}$ is also shown for the same model parameter values in Fig. 14(b) and (d). For small values of the plasticity, the diagrams have maximum which means that the plasticity has significant effect on the time variation of *X*. Comparison of Fig. 14(a) with Fig. 14(c) and Fig. 14(b) with Fig. 14(d) reveals that this behavior can be seen for wide range of self-renewal rates of CSCs and progenitor cells.

Now, we can also obtain sensitivity of the fraction and its time derivatives to the model parameters. Here, we obtain the time-dependent sensitivity of *X* to the plasticity (ρ_{ps}) as follows

$$\frac{\partial X}{\partial \rho_{ps}} = \frac{\partial \beta_1}{\partial \rho_{ps}} + \frac{\partial \beta_2}{\partial \rho_{ps}}\left(\frac{\exp(\alpha t) - \frac{\lambda}{A}}{\exp(\alpha t) + \frac{\lambda}{A}}\right) + \beta_2\left(\frac{2\exp(\alpha t)\left(t\frac{\partial \alpha}{\partial \rho_{ps}}\left(\frac{\lambda}{A}\right) - \frac{\partial\left(\frac{\lambda}{A}\right)}{\partial \rho_{ps}}\right)}{\left(\exp(\alpha t) + \frac{\lambda}{A}\right)^2}\right)$$

$$\Rightarrow \frac{\partial X}{\partial \rho_{ps}} = -\frac{1}{2a} + \sqrt{\frac{c}{a} + \kappa^2}\frac{2\exp(\alpha t)\left(t\left(\frac{\lambda}{A}\right)\frac{a(1-\kappa)}{\sqrt{a\gamma}} - \frac{2}{A^2}\frac{\partial \epsilon}{\partial \rho_{ps}}\right)}{\left(\exp(\alpha t) + \frac{\lambda}{A}\right)^2} \qquad \textbf{(2.18)}$$

$$+ \frac{1-\kappa}{2a\sqrt{\frac{c}{a} + \kappa^2}}\left(\frac{\exp(\alpha t) - \frac{\lambda}{A}}{\exp(\alpha t) + \frac{\lambda}{A}}\right)$$

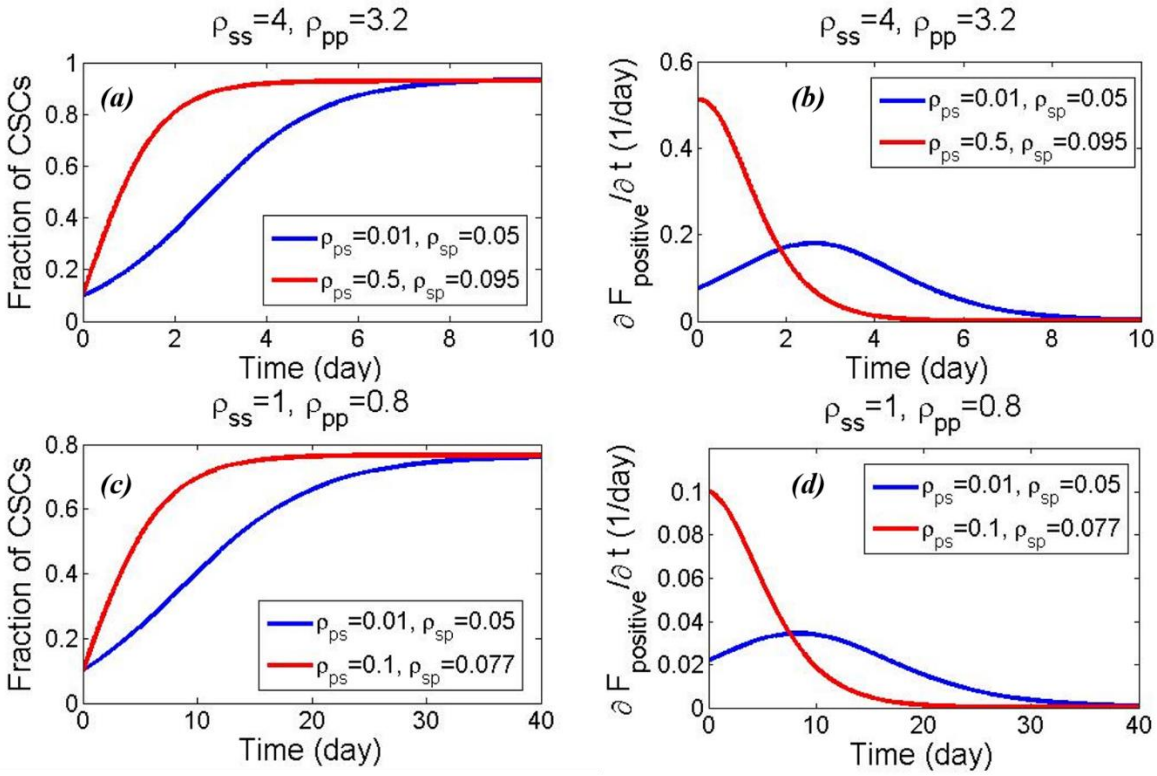

Figure 14 Time variation of fraction of CSCs (a) and (c), and its time derivative (b) and (d) for different model parameter values.

where

$$\epsilon = \frac{1}{\sqrt{\frac{c}{a}+\kappa^2}}(X_0-\kappa)$$
$$\Rightarrow \frac{\partial \epsilon}{\partial \rho_{ps}} = \frac{1}{2a\sqrt{\frac{c}{a}+\kappa^2}}\left(\frac{(1-\kappa)(x_0-\kappa)}{\frac{c}{a}+\kappa^2}-1\right) \quad \textbf{(2.19)}$$

The obtained sensitivity to ρ_{ps} is verified by checking its function at $t = 0$, that is equal to zero.

To clarify the sensitivity of *X* to the plasticity, we use Eq. (2.18) to obtain Fig. 15. Variation of $\partial F_{positive}/\partial \rho_{ps}$ nonlinearly depends on the plasticity. In the other word, there are local minimum and maximum for the sensitivity of *X* to the plasticity.

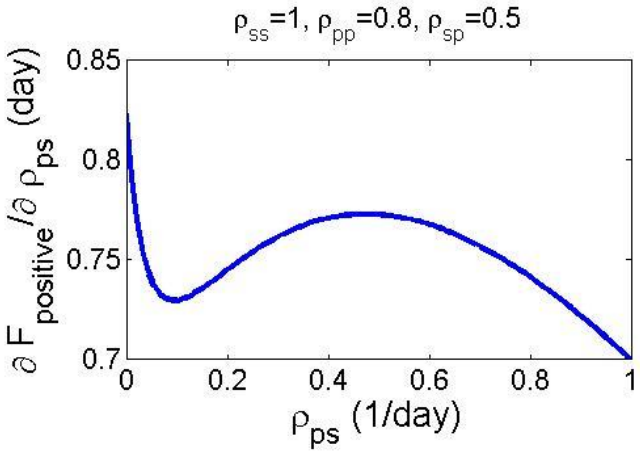

Figure 15 Sensitivity of *X* ($F_{positive}$) to the plasticity ρ_{ps}.

2.5 Discussion

In this part of the project, we study the theoretical modeling of phenotype switching within cancer cell populations, and compare the model results with experimental results done on large numbers of cells (Gupta et al. 2011). We highlight a deficiency present in experimental studies only based on the behavior of cancer cells in large populations. Specifically, the analysis of a large population of cells does not inherently provide sufficient information about the behavior of cancer cells to completely characterize what may be observed at different stages of tumor

growth and importantly, tumor initiation. That is, mathematically, the deterministic analysis as an average of observed random behavior of single cells conceals the stochastic properties of the system. To this end, we show that the stochastic behavior of cancer cells, as may be experimentally measured using the mammosphere formation assay, is not defined well by the deterministic or large population behavior of the system under consideration. We obtain parameters fitting the experimental data of Gupta et al. (2011) to the TCM presented in this work, and we show that multiple sets of parameters adequately describe the experimental, deterministic results, but because of changes in the cellular death rates and self-renewal rates, the stochastic properties of these parameter cases vary greatly. This analysis is also repeated using HM including different levels of negative cells and a positive compartment. Corresponding MFE and AMS are shown in Figs. 9 and 10. It is clearly shown that the stochastic behavior of cancer cells modeled using HM is more sensitive than the ones studied by TCM while they have almost the same behavior in large populations (validated by the experimental results in [9]). Hence, we can conclude that analysis of small population of cancer cells, using stochastic modeling, is as important as a study of large populations of cells, employing deterministic modeling. In addition, the modeling should be verified experimentally on both scales to be able to obtain a promising model and use it to estimate the behavior of cancer cells better than before.

The concept of plasticity in the cancer cell population and its importance on aggressiveness of tumors is also included in the theoretical modeling in this part of the project. We show that plasticity affects the survival probability of cancer cells, which in the steady state is representative of the MFE as well. However, this dependency may be influenced by other parameters such as death rates of the phenotypes, as shown in Fig. 10. That is, the contours depicted in Fig. 10 show that increasing plasticity may actually decrease the overall survival probability for certain cases of death rates of positive and negative cells. This suggests that clinically, if such behavior is indeed observed experimentally, carefully controlling death rates may be advantageous in certain cases of cellular plasticity to act to decrease overall cellular survival.

In addition, we analytically obtained the time dependent solution of fraction of CSCs and showed that its time variation depends on the plasticity. We could also attain the sensitivity of the result to the plasticity and illustrate that there are local minimum and maximum for the sensitivity of the fraction of CSCs to the plasticity.

Chapter 3
Mathematical analysis of experimental errors: effects of imperfectness of biomarkers in cancer study

In this chapter, a new phenomenological model is proposed to investigate the importance of experimental errors, as a result of imperfectness of biomarkers, in the study of cancer cell populations. Two limits of large and small populations of cells are considered. Stochastic analysis is used to investigate the behavior of cancer cells in the limit of low cell number. The master equation is written and solved numerically using Gillespie algorithm. The analytical solution is also provided using generating functions by considering reasonable approximations. We analyze the behavior of large populations of cancer cells using the average equations. We use both deterministic and stochastic analyses to determine the parameter values of the model based on the experimental data provided by Dr. Mani's group, MD Anderson Cancer Centre. Then, the model is utilized to investigate the effects of imperfectness of biomarkers on the stochastic and deterministic behavior of cancer cells. We show that the imperfectness may cause important errors in the study of cancer cells such as overestimation of real proportion of positive cells and underestimation of MFE, as a parameter representing the probability of forming cancer colonies. In addition to the effect of imperfectness, some predictions are presented to show the errors caused by inconsistencies in the time period of culturing in MFA experiments. We also provide the analytical solution of the PDE which is obtained for the corresponding generating function. The solution reveals that it is possible to control the survival probability of positive cells by changing the self-renewal rate of negative cells, even in a more effective way than the direct change of the self-renewing capacity of positive cells.

3.1 Introduction

The main focus of this chapter is the effect of imperfectness on the stochastic behavior of cancer cells. Stochastic analysis can be used widely in interpreting and modeling natural and synthetic phenomena whenever randomness comes into the picture. Stochastic analysis has been used to model the initiation and progression of cancer since mid-19th century. The variation in the number of spleen colony-forming cells per colony was studied by Till et al.

(1964) to propose that hematopoietic stem cells (HSCs) may be mathematically modeled by a "birth-and-death" process. The experimental measurements showed that the birth-and-death process is an appropriate model of HSC proliferation that resulted in the idea of stem cell division involving randomness. The cancer stem cell hypothesis, initially proposed for hematopoietic cancers [2], [32], helped to use the models and theories developed for HSCs also in the area of cancer biology. In this hypothesis, it is assumed that the so called cancer stem cells (CSCs) are the small population in any tumor with almost unlimited capacity of self-renewal and long time-period of survival with respect to the other cells in the population. Another example of this is the birth-and-death process used in the radiation therapy modeling [33].

Different phenomenological models have been developed during the last decade to study the initiation and proliferation of cancer cells [9], [34], experimental procedures in cancer biology, and therapeutic procedures [35], [36]. Gupta et al. (2011) assumed that the proliferation of cancer cells is random and a Markov process is an appropriate method to model it. The detail of experimental procedures and how they can be modeled are other important factors which should be taken into consideration in the development of a model. We use proportion of positive cells and MFE as two parameters in the study of cancer cell populations. The proportion of positive cells can be obtained using an experiment in which the initial cell population is usually bigger than 10^5 cells [9]. This experiment can be modeled deterministically without losing any accuracy. Mammosphere formation efficiency is another parameter, which can be obtained using MFA. The start of the experiment is for example 1000 separate cancer cells that start to grow and some of them survive and make colonies. To model this experiment, individual cells should be considered and thus we are dealing with small populations of cells. Therefore, stochastic analysis should be used to model this experiment because of the low number of cells.

A new phenomenological model is proposed in this chapter with the main purpose of investigating the imperfectness of biomarkers, e.g., imperfectness in recognizing the cell phenotypes in cancer cell populations. Identification of different cell phenotypes and the

degree of plasticity are important in the study of cancers and the design of suitable therapies. Experimentalists have studies this problem and have designed experiments so that the obtained results became more accurate [37]. Our results and analysis clarify the importance of paying attention to the results of these errors and trying more to eliminate them. In addition, after more experimental validation, the model may be used as a filtration method for the experimental data to eliminate the error of imperfectness of biomarkers. We analyzed the effect of considering or eliminating plasticity in the switching between different cell types as well. We show that the effect of imperfectness of biomarkers can be as important as the effect of existence of plasticity.

3.2 Method

A phenomenological model is used in this chapter to investigate the effect of imperfectness of biomarkers on the study of CSCs. The purpose of the model is to study this imperfectness in recognizing real CSCs in both positive and negative biomarker cells. Hence, we consider the cancer cell population includes two populations of positive and negative cells. However, what we recognize using biomarkers are different from reality because of their imperfectness. It means that some of the positive cells are actually progenitors and some of the negative cells are real CSCs [38]. Thus, some post-processing should be applied on the experimental data to filter errors of the experiments and obtain the actual data with the lowest possible error. Therefore, we use a new phenomenological model in this chapter to show the importance of investigating imperfectness of biomarkers.

The proposed model includes four compartments of real cancer stem cells (A), fake cancer stem cells (B), fake progenitors (C), and progenitors (D) (Fig. 16). Each compartment is capable of self-renewing and switching to other compartments. The death is also included for each compartment (Fig. 16). The definitions of the parameters, shown in Fig. 16, are presented in Table 9.

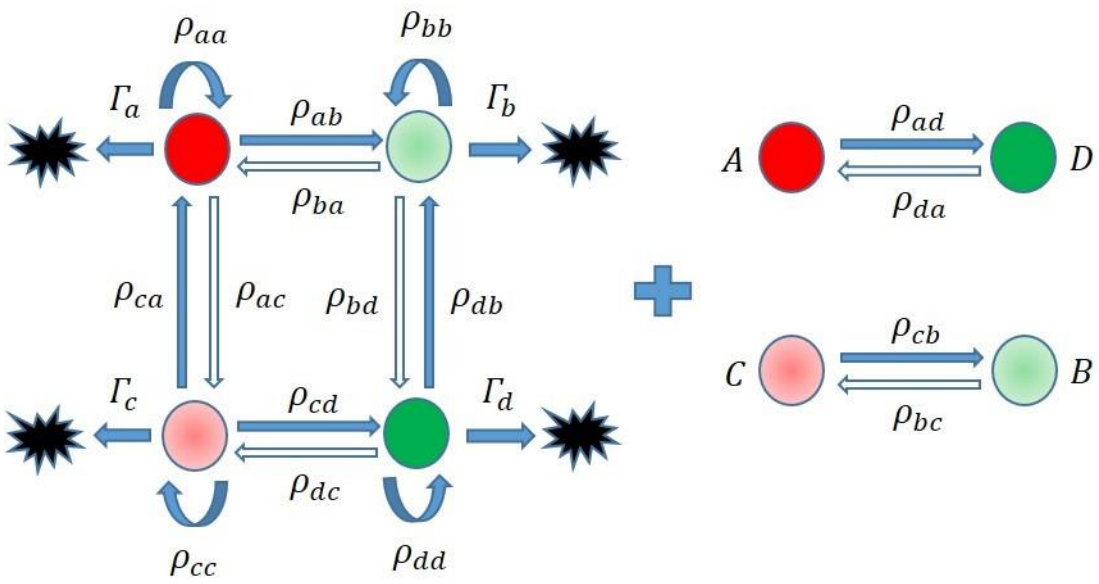

Figure 16 Schematic representation of the imperfect biomarker model. The parameters shown here are described in Table 9. Bold red and green circles are real CSCs and progenitor cells, respectively. Pale red and green circles are fake progenitor cells and CSCs, respectively.

The proposed model is developed for two limits of low and high number of cells. Cancer cell growth and switching between different compartments, e.g., different phenotypes in the biological context, can be modeled deterministically for large population of cells while stochastic analysis should be employed to study the behavior of the system with low number of cells. It is based on the fact that individual cells behave randomly and we have to consider this randomness in our analysis. Therefore, some quantitative data, such as survival rate, cannot be captured using the deterministic analysis. Therefore, both deterministic and stochastic mathematical modeling are presented here for the four compartment model and used to validate the model and obtain new theoretical results.

Table 9 Definition of the parameters of the imperfect biomarker model.

Parameter	Description
ρ_{kk}	Rate of self-renewal of compartment K
$\rho_{kl}, k \neq l$	Rate of mutation of compartment K to compartment L
Γ_k	Death rate of compartment K

3.2.1 Deterministic modeling

The deterministic mathematical modeling includes logistic growth of the cancer cells and linear transitions between different compartments. Time variation of the population of each cancer cell phenotype, shown as different compartments in Fig. 16, can be given as the following ordinary differential equations

$$\begin{aligned}
\frac{dA}{dt} &= (\rho_{aa} - \Gamma_a)A\left(1 - \frac{A+C}{K_P}\right) + \sum_{k(k\neq a)} (\rho_{ka}K - \rho_{ak}A) \\
\frac{dB}{dt} &= (\rho_{bb} - \Gamma_b)B\left(1 - \frac{B+D}{K_N}\right) + \sum_{k(k\neq b)} (\rho_{kb}K - \rho_{bk}B) \\
\frac{dC}{dt} &= (\rho_{cc} - \Gamma_c)C\left(1 - \frac{A+C}{K_P}\right) + \sum_{k(k\neq c)} (\rho_{kc}K - \rho_{ck}C) \\
\frac{dD}{dt} &= (\rho_{dd} - \Gamma_d)D\left(1 - \frac{B+D}{K_N}\right) + \sum_{k(k\neq d)} (\rho_{kd}K - \rho_{dk}D)
\end{aligned} \qquad \textbf{(3.1)}$$

where *A*, *B*, *C* and *D* are average density of the corresponding compartments in the cancer cell population. Carrying capacity for the positive and negative cells are also shown by K_P and K_N (equal to 10^5), respectively. The other parameters used in Eq. (3.1) are shown in Table 9. It should be noted that *K* can be any compartment except the one determined in each equation (Eq. (3.1)).

The results of the model should be validated using the experimental results to obtain relevant parameter values. One of the usual experimental data in the context of cancer stem cell biology is the proportion of CSCs [9]. The result of this experiment is related to the large cell population that can be mathematically modeled by deterministic solution. The fake and real proportion of positive cells can be defined as follows based on the definition of each compartment in the imperfect biomarker model (Fig. 16).

$$X_{real} = \frac{A+C}{A+B+C+D}, X_{fake} = \frac{A+B}{A+B+C+D} \qquad \textbf{(3.2)}$$

where X_{real} and X_{fake} are the proportion of real and fake CSCs, respectively. Therefore, solving set of ODEs for different compartments in the model (Eq. (3.1)) gives not only time-dependent number of cells in each compartment but also the real and fake proportion of positive cancer cells versus time.

3.2.2 Stochastic modeling

In the limit of small number of cells, taking average and using deterministic modeling is not useful in the survival analysis of CSCS, which is equivalent to MFE in the experimental data. For example, if we consider a single cell with self-renewal rate bigger than the other rates for that cell, it certainly grows toward becoming a big tumor. However, stochastic analysis tells us that even in this case we may have no cell after a while (because of the possibility of sudden death of the cells). Mammosphere formation assay is among the experiments dealing with small cell numbers in a period of culturing. In this assay, usually single cancer cells will be put in separate places in a suitable environment and allowed to grow. Hence, each of these single cells may grow and form colonies of cancer cells or die after a while. The rates of growth of the colonies are not the same. Therefore, number of spheres, colonies greater than a cutoff size, will be counted after certain number of days. This data can tell us the probability of forming tumor from initial cancer cells, or risk of tumor initiation from initial cancer cells, in the body. Therefore, we use the stochastic analysis of the imperfect biomarker model to study the effect of imperfectness in the low cell number limit.

The stochastic modeling of cancer cell proliferation has been developed by considering the divisions and switching between different phenotypes as a Markovian process [9]. In any Markov process, future of the process can be predicted only based on its present condition. Therefore, the master equation of the imperfect biomarker model (Fig. 16) can be written as follows based on this assumption.

$$\frac{\partial \boldsymbol{p}}{\partial t} = \sum_{k} \alpha_{kk}(n_K - 1)\boldsymbol{p}(n_K - 1, t) + \sum_{k,l(k\neq l)} \rho_{kl}(n_K + 1)\boldsymbol{p}(n_K + 1, n_L - 1, t)$$
$$+ \sum_{k} \beta_k(n_K + 1)\boldsymbol{p}(n_K + 1, t) - \sum_{k} \alpha_{kk} n_K \boldsymbol{p}(\boldsymbol{t}) \qquad \textbf{(3.3)}$$
$$- \sum_{k,l(k\neq l)} \rho_{kl} n_K \boldsymbol{p}(t) - \sum_{k} \beta_k n_K \boldsymbol{p}(t)$$

where the probability of being at state $p(n_A, n_B, n_C, n_D, t)$ is defined as $\boldsymbol{p}(t)$. The parameters $\alpha_{ii}, i = a, b, c, d$and $\beta_i, i = a, b, c, d$ are also defined as

$$\alpha_{ii} = \sum_{j} \delta_{i,j}\rho_{jj}\left(1 - \frac{(\delta_{1,j} + \delta_{3,j})(n_1 + n_3)}{K_P} - \frac{(\delta_{2,j} + \delta_{4,j})(n_2 + n_4)}{K_N}\right)$$
$$\beta_i = \sum_{j} \delta_{i,j}\Gamma_j\left(1 - \frac{(\delta_{1,j} + \delta_{3,j})(n_1 + n_3)}{K_P} - \frac{(\delta_{2,j} + \delta_{4,j})(n_2 + n_4)}{K_N}\right) \qquad \textbf{(3.4)}$$

based on the logistic growth modeling. One should note that Eqs. (3.1) have written based on phenomenological extension of mass-action laws, however, they can be obtained from the above master equation with appropriate approximations. . In order to show the probability of being in other states, the difference of the state from $p(n_A, n_B, n_C, n_D, t)$ is just shown, such as $\boldsymbol{p}(n_A - 1, t)$ which shows the probability of being at state $p(n_A - 1, n_B, n_C, n_D, t)$.

The obtained master equation (Eq. (3.3)) can be solved utilizing the Gillespie algorithm. The results of Gillespie algorithm are the average of 100 runs which have been done by MATLAB 12.

In the stochastic analysis, for the time periods when the number of cells is so small, $(n_1 + n_3)/K_P \ll 1$ and $(n_2 + n_4)/K_N \ll 1$, the logistic model can be approximated to be linear. Hence, the parameters in Eq. (3.4) will be equal to $\alpha_{ii} = \sum_j \delta_{i,j}\rho_{jj}$ and $\beta_i = \sum_j \delta_{i,j}\Gamma_j$. The formulas obtained for analytical solutions are derived using this approximation while the logistic model is used for numerical solution of master equation (Eq. (3.3)).

Each compartment in the imperfect biomarker model has separate survival probabilities; we can obtain survival probability of real or fake CSCs as well as non-CSCs. This important parameter can be obtained using the generating function $\boldsymbol{F}(t) = \sum_{n_A=0}^{\infty}\sum_{n_B=0}^{\infty}\sum_{n_C=0}^{\infty}\sum_{n_D=0}^{\infty} z_A^{n_A}\, z_B^{n_B}\, z_C^{n_C}\, z_D^{n_D}\, \boldsymbol{p}(t)$. Taking derivatives of both sides of this relation and substituting $\partial \boldsymbol{p}(t)/\partial t$ from Eq. (3.3) result in the following partial differential equation.

$$\frac{\partial \boldsymbol{F}(\boldsymbol{t})}{\partial t} = \sum_{k} z_K \rho_{kk}(z_K - 1)\frac{\partial \boldsymbol{F}(\boldsymbol{t})}{\partial z_K} + \sum_{k,l(k\neq l)} z_K \rho_{kl}(z_K^{-1} z_l - 1)\frac{\partial \boldsymbol{F}(\boldsymbol{t})}{\partial z_K} + \sum_{k} z_K \Gamma_k (z_K - 1)\frac{\partial \boldsymbol{F}(\boldsymbol{t})}{\partial z_K}. \quad \textbf{(3.5)}$$

The survival probability should be obtained as $t \to \infty$, e.g., at the steady state condition. Hence, time derivative is setting to be equal to zero. Therefore, the steady state solution of $z_k, k = a, b, c, d$ can be obtained using the following equations, by considering Eq. (3.5) in the steady state condition.

$$\begin{gathered}
\rho_{aa}(z_A - 1) + \rho_{ab}\left(z_B z_A^{-1} - 1\right) + \rho_{ac}\left(z_C z_A^{-1} - 1\right) + \rho_{ad}\left(z_D z_A^{-1} - 1\right) \\
+\Gamma_a\left(z_A^{-1} - 1\right) = 0 \\
\rho_{bb}(z_B - 1) + \rho_{bd}\left(z_D z_B^{-1} - 1\right) + \Gamma_b\left(z_B^{-1} - 1\right) = 0 \\
\rho_{cc}(z_C - 1) + \rho_{ca}\left(z_A z_C^{-1} - 1\right) + \rho_{cb}\left(z_B z_C^{-1} - 1\right) + \rho_{cd}\left(z_D z_C^{-1} - 1\right) \\
+\Gamma_c\left(z_C^{-1} - 1\right) = 0 \\
\rho_{dd}(z_D - 1) + \rho_{db}\left(z_B z_D^{-1} - 1\right) + \Gamma_d\left(z_D^{-1} - 1\right) = 0
\end{gathered} \quad \textbf{(3.6)}$$

The set of equations for $z_A, k = A, B, C, D$ (Eq. (3.6)) can be solved analytically to obtain different solutions of these variables. The extinction probability that is equal to "1-survival probability" can be obtained using the following definition

$$p_{extinction}(K) = z_K, \text{ K=A, B, C, D} \quad \textbf{(3.7)}$$

where we start the simulation with single *K* cells. Therefore, those solutions with $0 \leq z_K \leq 1, k = A, B, C, D$ are only acceptable.

3.2.3 Stochastic sensitivity analysis

We study the sensitivity of the imperfect biomarker model to different parameter values as well. The sensitivity of the stochastic model to the model parameters can be obtained analytically. Although this analysis is useful and theoretically important, we use numerical sensitivity analysis to make the procedure easier. The dependency of the studied stochastic variables on the parameter values is obtained numerically by solving the master equation (Eq. (3.3)). This analysis is shown later.

3.3 Results

We show the significant effects of imperfectness on two limit of small and large cancer cell populations using the proposed imperfect biomarker model. The proportion of cells or other parameters related to the experiments with large population of cells are obtained using the deterministic analysis. Mammosphere formation efficiency and the other random results are also attained employing stochastic analysis.

In addition to the imperfectness of biomarkers, we present another important result related to the concept of plasticity in cancer cell population [9], [40]. We show that non-zero steady state value of the real-proportion of positive cells can be obtained even without considering plasticity in the model. In the work of Zapperi et al. (2012), it has been suggested to model the imperfectness of biomarkers and consider the effects of plasticity. However, their model includes all possible switching between the cell types of the population without any restriction based on the biological criteria.

3.3.1 Parameter determination

In this chapter, experimental results provided by Mani's group are used to obtain the parameters of the model (Fig. 16). The comparison of the theoretical and experimental results (Fig. 17) shows that the proposed imperfect biomarker model is capable of capturing the biological behavior of cancer cells. There are some important assumptions behind the analysis of the model including: 1) plasticity rates are considered to be zero($\rho_{ba} = \rho_{bc} = \rho_{da} = \rho_{dc} = 0$); 2) rate of producing fake CSCs and progenitor cells from real ones are so small

($\rho_{ab} = \rho_{ac} = \rho_{db} = 0.01$); 3) the correspondent rates for real and fake compartments are considered to be the same ($\rho_{cb} = \rho_{ab}, \rho_{cc} = \rho_{aa}, \rho_{cd} = \rho_{ad}, \rho_{dd} = \rho_{bb}$); 4) the initial proportion of fake cells are considered to be 1% of the population. The initial cells are randomly chosen in the Gillespie algorithm. If the random number is between *0* and *0.01* it is fake progenitor and if it is between *0.01* and *1* it is real progenitor cell, because negative cancer cells used to obtain the experimental results. The parameters of the model are obtained based on these assumptions (Table 10). Henceforth, except the situations in which other values are mentioned for the parameters, we use these values. In addition, the time at which the results are obtained are considered to be at day 6, the final time at which the experimental results are reported, unless other days are mentioned.

The fake proportion of positive cancer cells is obtained as a function of time using Eq. (3.2) for both normoxic and hypoxic conditions (Fig. 17(a)). It is shown that the conditions in which the cancer cells grow (microenvironmental condition) may affect both time-dependent and steady state values of the fake proportion of positive cells in the experiments. Theory predicts that the time the populations need to reach the steady state varies by changing the microenvironmental conditions. In addition, hypoxic condition (low oxygen concentration) causes the system to finally have larger fraction of biomarker positive cells (Fig. 17).

We use Gillespie algorithm as a numerical solution of master equation (Eq. (3.3)) to obtain the suitable parameters corresponding to the experimental values of MFE (Fig. 17(b)). Our results show that the experimental and theoretical results at day 6 are so close and MFE is smaller for the population under hypoxic condition. They also show that the number of mammospheres increases by growing time (Fig. 17(b)). The steady state value of MFE oppositely predicts that MFE becomes larger under hypoxic condition. Hence, the number of days of experimentation is really important if we want to compare MFE for the cancer cells under different conditions. The conditions should be provided so that the cancer cells grow separately for enough time and MFE reaches to its steady state value.

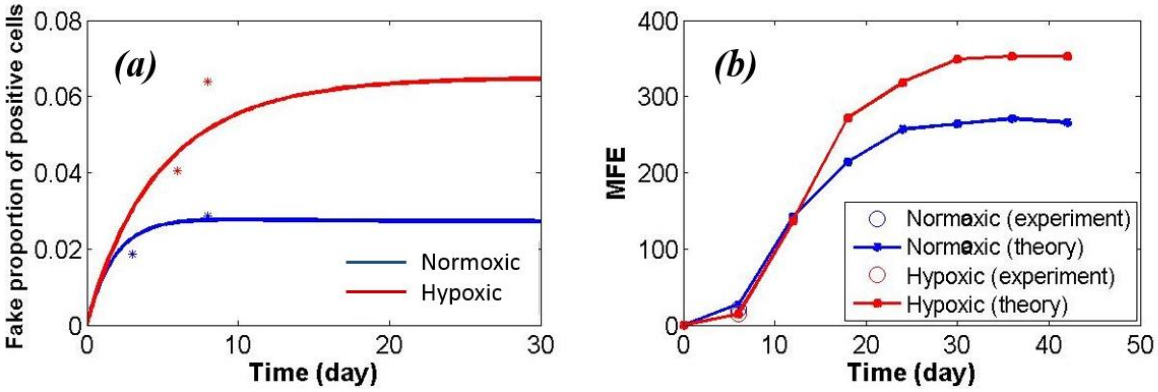

Figure 17 Comparison of theoretical and experimental results provided by Dr. Mani's group at MD Anderson Cancer Centre. (a) Proportion of positive cells (starting from 10^5 negative cells) and (b) mammosphere formation efficiency for the cancer cells in normal and hypoxic (low oxygen) conditions (the initial condition of both experimental and modeling is 1000 single negative cells).

Table 10 Parameters of the imperfect biomarker model obtained to fit the experimental results provided by Dr. Mani's group at MD Anderson Cancer Centre. The numbers in the parentheses are standard deviation and the other ones are the averages.

Mic. Cond.	ρ_{aa}	ρ_{ad}	ρ_{bb}	ρ_{bd}	ρ_{ca}	Γ_a	Γ_b
Normoxic	0.74(0.14)	0.45(0.12)	0.63(0.08)	0.46(0)	0.58(0.21)	0.15(0.12)	0.46(0.08)
Hypoxic	0.93(0)	0.78(0)	0.48(0)	0.16(0)	0.46(0.21)	0.01(0)	0.31(0)

3.3.2 Deterministic results (limit of large cell number)

Proportion of positive cells and population doublings are among the parameters can be obtained experimentally using large population of cells. The population doublings is a parameter shows that how fast the population of cells grows. It is defined as $log(N/N_i)/log(2)$ where N and N_i are the current and initial number of cancer cells, respectively.

We use the same parameters and the conditions to obtain both fake and real proportion of positive cells in Fig. 17(a) and 18, respectively. The real proportion is much less than the fake

proportion. In addition, real proportion converges slower to its steady state value for both normal and hypoxic conditions. Hence, the imperfect biomarker model shows that by the considered conditions, such as no plasticity, real proportion of positive cells may be much less than what is obtained in the experiment.

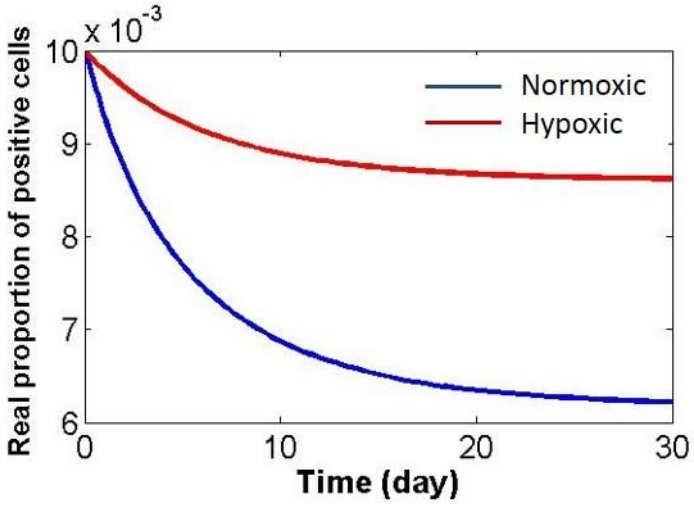

Figure 18 Real proportion of positive cells corresponding to the parameters used to obtain Fig. 2 (a) for fake proportion of positive cells (starting from 10^5 negative cells).

In the imperfect biomarker model, non-zero rates of $\rho_{ba} = \rho_{da}$ and/or $\rho_{bc} = \rho_{dc}$ is equal to including plasticity in our theoretical study. Non-zero values of plasticity rates ρ_{ba} and/or ρ_{bc} change the fake and real proportion of positive cells so that their differences decrease dramatically for both normoxic and hypoxic conditions (Fig. 19). The difference of the real and fake proportions $X_{fake} - X_{real}$ is almost independent of ρ_{da} which is the plasticity rate to real CSCs under normoxic conditions while it is changed under hypoxic condition more than 30% (Fig. 19(a)). The effect of ρ_{dc} is much more than the effect of ρ_{da} and higher rates causes $X_{fake} - X_{real}$ to become negative, e.g., real proportion becomes larger than the fake proportion. It is also clear that the dependency of $X_{fake} - X_{real}$ on ρ_{dc} is almost the same for the cancer cell populations under both normoxic and hypoxic conditions.

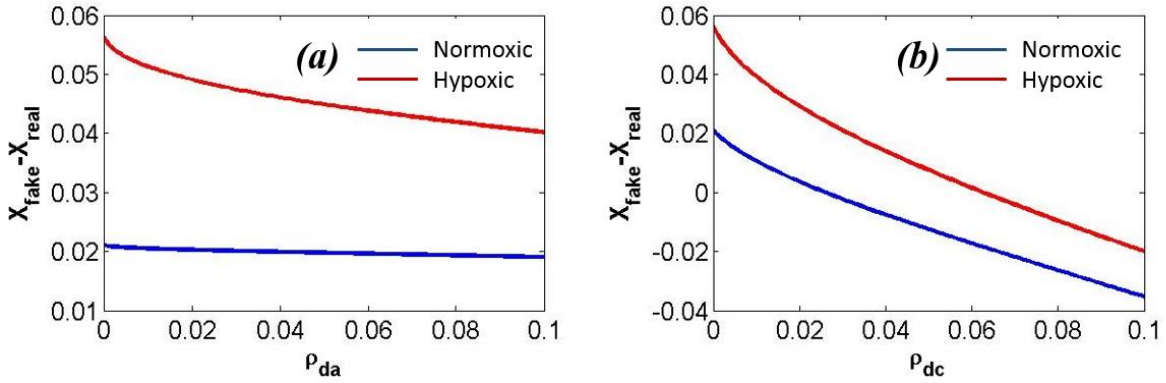

Figure 19 Difference of fake and real proportions of positive cells versus plasticity rates $\rho_{ba} = \rho_{da}$ (plasticity to real CSC) (a) and $\rho_{bc} = \rho_{dc}$ (plasticity to fake progenitor cell) (b) (starting from 10^5 negative cells).

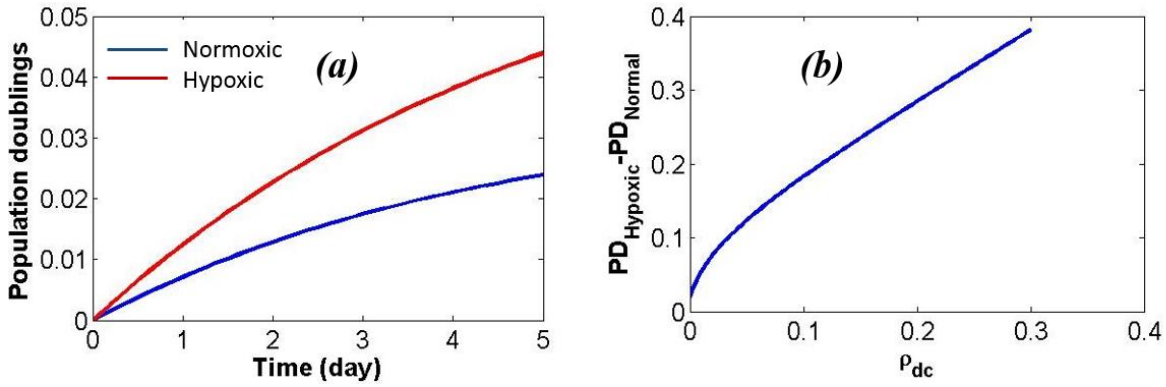

Figure 20 (a) Population doublings of the cancer cells under both normoxic and hypoxic conditions and (b) its difference under these microenvironmental conditions versus plasticity rate ρ_{dc} (starting from 10^5 negative cells).

Variation of population doublings (*PD*) of cancer cells with respect to time is also shown in Fig. 20(a). This figure shows that the population of cancer cells grows faster under hypoxic conditions based on the presented mathematical modeling. However, the growth rate seems to be slow that also reflects the considered carrying capacity and logistic growth in the modeling.

We also investigate the effect of plasticity on the population doublings to show the effect of ρ_{dc} on *PD* for the cancer cell populations under normoxic and hypoxic conditions (Fig. 20(b)).

It is clearly shown that $PD_{hypoxic} - PD_{normoxic}$ increases by increasing ρ_{dc}. The plasticity rate ρ_{da} has also the same effect on the difference of *PD*.

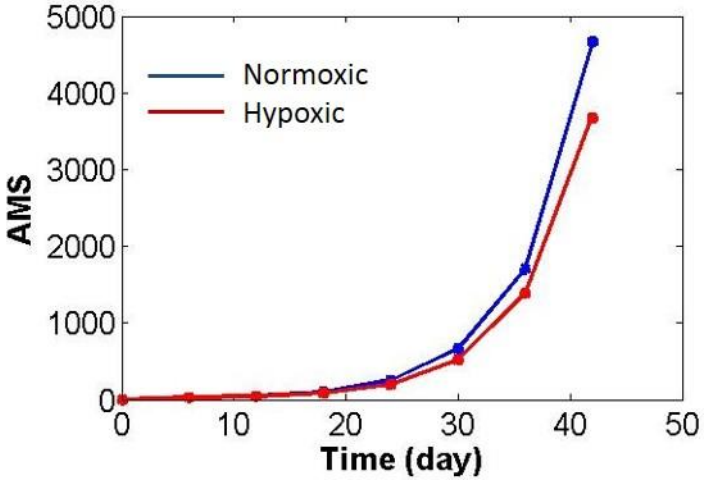

Figure 21 Average size of the mammospheres versus time for the cancer cell populations under normoxic and hypoxic conditions corresponding to the mammospheres with MFE presented in Fig. 2 (b) (the initial condition of stochastic modeling is 1000 single negative cells).

3.3.3 Stochastic results (limit of low number of cells)

We also tried to capture the stochastic behavior of cancer cells employing the proposed imperfect biomarker model. Average mammosphere size, which corresponds to the illustrated MFE in Fig. 17(b), is presented in Fig. 18 for the cells under both normoxic and hypoxic conditions. The cells exponentially grow under both microenvironmental conditions so that the average growth rate between days 20 and 40 is more than 30 times of the average growth rate in the first 20 days. Average mammosphere size under normoxic condition is bigger than the AMS under hypoxic conditions after day 10 (Fig. 21). However, it is in opposite way for the lower time stages. By comparing the diagrams of Figs. 17(b) and 21, we can conclude that in the conditions that the MFE is higher AMS is lower.

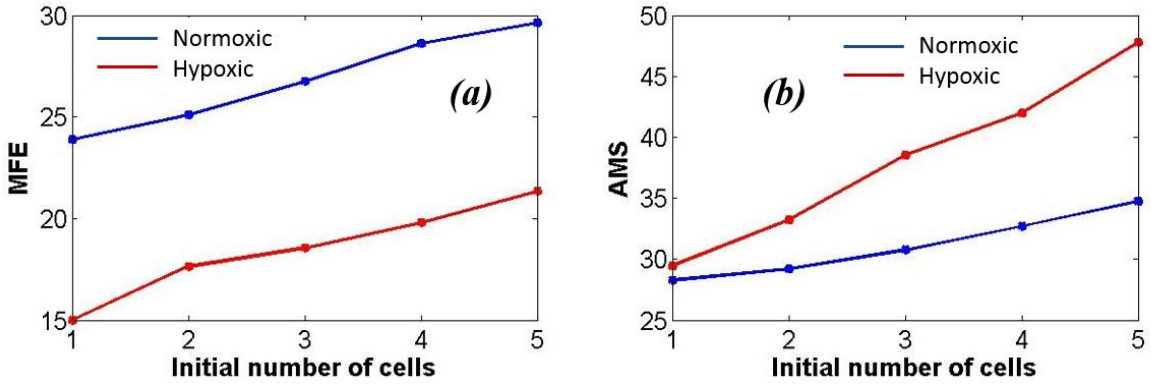

Figure 22 Variation of MFE (1000 separate groups of cells initially considered in the analysis using Gillespie algorithm) (a) and AMS (b) with respect to the initial number of cells in each initial group of cells in MFA.

Previously, it was mentioned that in the MFA, single cells are grown to form mammospheres. However, it is possible to culture groups of cells that are initially made of more than one cell. The initial condition of a stochastic process like this affects the behavior of the system as shown in Fig. 22. It can be seen that by increasing the initial number of cells in each group, number of mammospheres increases. Moreover, the average size is also larger if there are more initial cells in each group. Effect of initial number of cells is almost the same on MFE for the cancer cells under both normoxic and hypoxic conditions. However, increase in the size of the mammospheres under hypoxic condition is approximately 3 times more than the mammospheres under normoxic conditions (in the considered range in Fig. 12(b)).

The diagrams of Fig. 22 are shown by assuming that the imperfectness of the initial population is *0.01*. In other word, the initial cells are chosen from a population of negative cells. However, there is a fraction of cells in this population that is actually positive and it is considered to be *0.01* in Fig. 22. This imperfectness may vary in different experiments and can be less or more than the considered fraction. Hence, the effect of increasing the initial imperfectness, imperfectness in the initial chosen cells, on number of mammospheres and their average size are obtained (Fig. 23). The imperfectness in the initial population of cancer cells is considered to be between *0.05* and *0.5*. Number of mammospheres that formed under both normoxic and hypoxic conditions increases by increasing the initial imperfectness (Fig. 23(a)). The effect of

imperfectness on cancer cells under hypoxic condition is more than its effect on cancer cells under normoxic condition. It causes higher MFE for the cells under hypoxic condition at day 6 (Fig. 23(a)). The effect of the imperfectness on MFE seems to be an important parameter. On average, *10-20* mammospheres will be added by *10%* increase in the initial imperfectness. Therefore, the stochastic analysis shows that imperfectness should be considered as an important parameter to compare the results of MFA in different experiments and draw any conclusion from the behavior of cancer cells in this experiment.

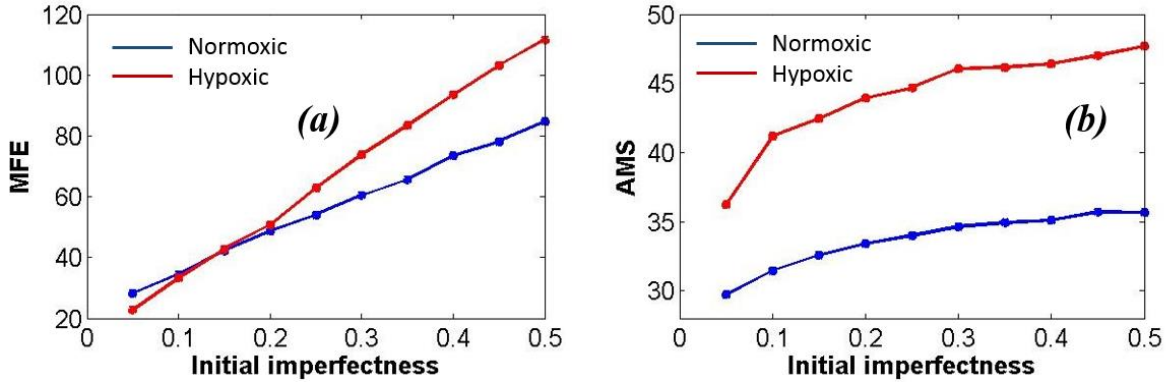

Figure 23 Effect of imperfectness in the population of cancer cells, the initial single cells are chosen from, on MFE (a) and AMS (b). The initial cells for the MFA is chosen from a population of negative cancer cells (based on the results of Dr. Mani's group) and the initial imperfectness is the fraction of this population that is actually positive cell (the initial condition of stochastic modeling is 1000 single negative cells).

In addition to the effect of plasticity on deterministic behavior of the cancer cells, plasticity can have an effect on their stochastic behavior. In order to show this effect, variations of MFE and AMS with respect to the two plasticity rates ρ_{da} and ρ_{dc} are illustrated in Fig. 24. Increasing plasticity rates increases the probability of forming mammospheres that represents the possibility of forming cancer colonies. In addition to the increase in number of mammospheres, their size also increases by increasing the plasticity (Fig. 24). It means that plasticity causes the initial mutated cells to form more colonies with larger sizes. This effect suggests that plasticity increases the aggressiveness of the tumors which is in agreement with the results of Chaffer et al. (2013). We also show that the effect of plasticity on the cancer cells

under hypoxic conditions is more than its effect on cancer cells under normoxic condition. Therefore, controlling the effect of plasticity for cancer cells under hypoxic conditions can be effective in therapeutic procedures based on the stochastic analysis of the model.

As it is shown in Fig. 24, the effects of plasticity rates ρ_{da} and ρ_{dc} are almost the same. Therefore, the experimental errors, which are based on the imperfectness of biomarkers to recognize different kind of cancer cells in the population, causes underestimation of the tumor formation probability and its growth rate significantly. By an exaggerated example, the importance of this parameter can be clarified: let us consider an imaginary experiment in which we recognize most of the cancer cells to be negative while there exists high imperfectness. By growing time, the negative cells may switch to the positive ones and we still recognize them as negative cells. Hence, we do not understand how much plasticity plays a role in this experiment.

3.3.4 General analytical study (stochastic analysis)

We also analyze the stochastic model analytically to investigate the behavior of the proposed imperfect biomarker model. Hence, instead of the parameters obtained for the model in Table 10, arbitrary variables are used. Equations (3.6) and (3.7) can be used to obtain the survival probability of each compartment in the model. The analytical solution of Eq. (3.6) results in the following functions for the steady state condition.

$$Z_A = Z_C = \frac{(\Gamma_a + \rho_{aa} + \rho_{ad}) - \sqrt{\rho_{aa}\left((\Gamma_a + \rho_{aa} + \rho_{ad})^2 \rho_{bb} - 4\rho_{aa}(\Gamma_b \rho_{ad} + \Gamma_a \rho_{bb})\right)}}{2\rho_{aa}\rho_{bb}} \qquad \textbf{(3.8)}$$

$$Z_B = Z_D = \frac{\Gamma_b}{\rho_{bb}}$$

where survival probabilities are $1 - z_K$. These are the only acceptable results among the sets of solutions of Eq. (3.6). The following assumptions are also used to obtain Eq. (3.10):

$$\rho_{cc} = \rho_{aa};\ \rho_{dd} = \rho_{bb};\ \rho_{cd} = \rho_{ad};\ \Gamma_a = \Gamma_c;\ \Gamma_b = \Gamma_d \qquad \textbf{(3.9)}$$

and all other parameters are considered to be zero.

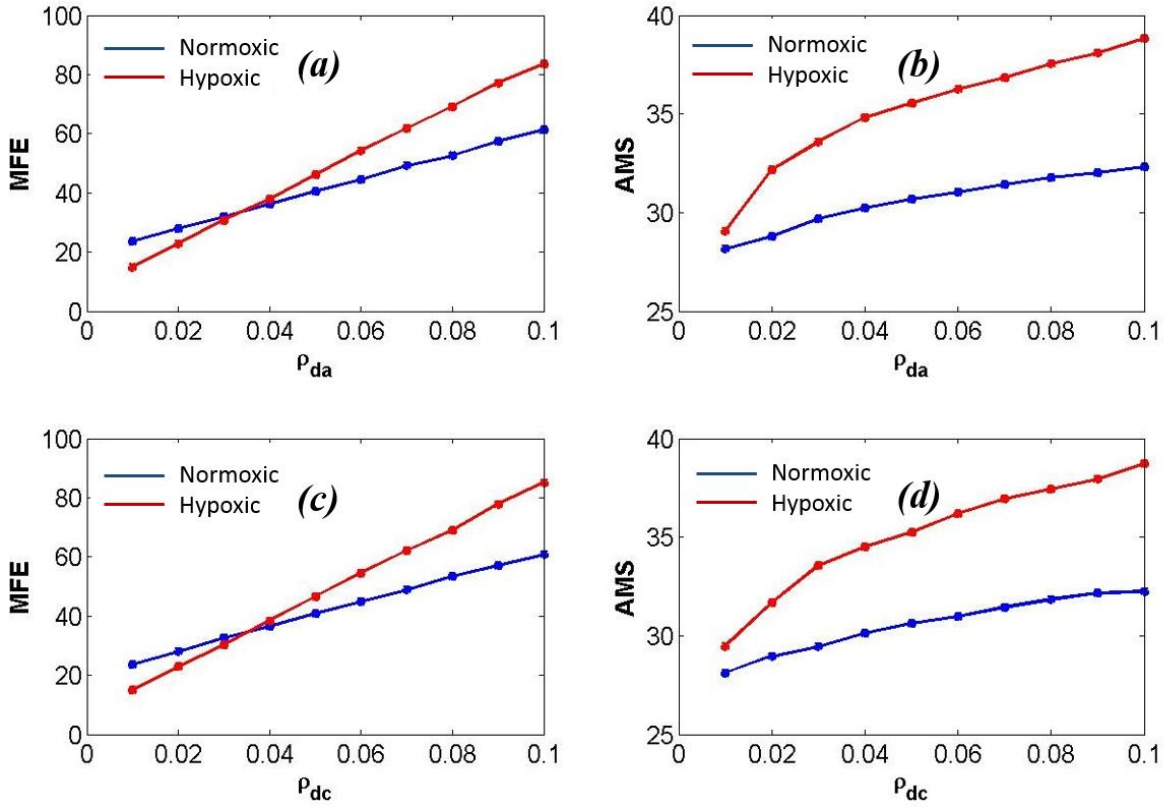

Figure 24(a) Variation of MFE with respect to ρ_{da}; (b) Variation of AMS with respect toρ_{da}; (c) Variation of MFE with respect toρ_{dc}; (d) Variation of AMS with respect to ρ_{dc} (the initial condition of stochastic modeling is 1000 single negative cells).

Steady state values of z_B and z_D depend only on self-renewals and death rates of negative compartments (B and D). Hence, extinction and survival probability p_{surv} of these compartments also just depend on the values of these parameters and do not depend on the switching rates and the rate of divisions related to the positive cells (compartments A and B). Nevertheless, survival probability of positive cells that is equal to $1 - z_A = 1 - z_C$ depends not only on ρ_{aa} and Γ_a but also on the self-renewal and death rates of negative cells. Interestingly the effect of ρ_{bb} on the survival probability of positive cells is more than ρ_{aa} which can be concluded by comparison of Fig. 25(a) and (b). We can see that increasing both $\rho_{aa}$and ρ_{bb} increases the survival probability of positive cells. In the considered range of parameters, p_{surv} almost linearly changes with respect to ρ_{aa} while its dependency on ρ_{bb} is nonlinear (Fig. 25). It is shown that the most effective range of ρ_{bb} is between *0.2* and *0.6*.

Hence, little increase in this range causes large effect on p_{surv}. Therefore, we can control the survival probability of positive cells effectively by controlling the self-renewal rate of negative cells that is an interesting analytical prediction which we hope will be verified experimentally in future.

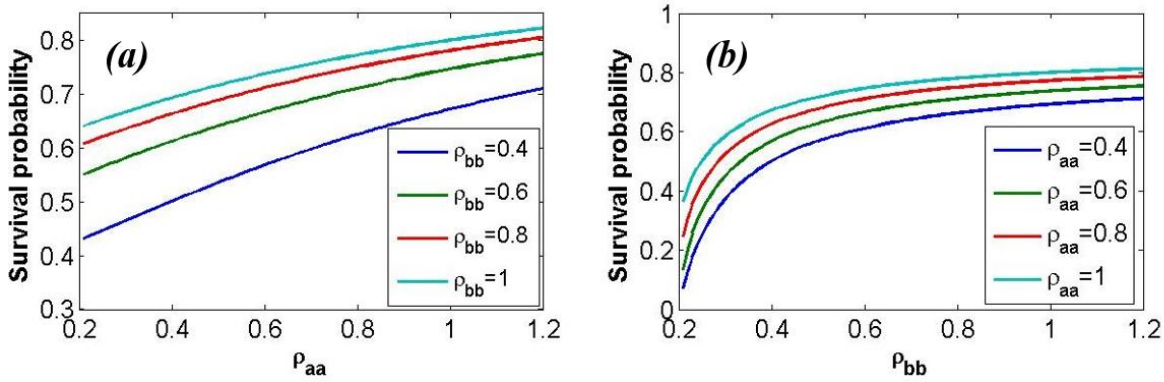

Figure 25 Survival probability of positive cells with respect to the values of the self-renewal rates ρ_{aa} (a) and ρ_{bb} (b). The other non-zero parameters of the model are considered to be:$\rho_{ad} = 0.5, \Gamma_a = \Gamma_b = 0.2$.

3.4 Discussion

We used stochastic and deterministic analyses to formulate the proposed imperfect biomarker model and study the behavior of small and large numbers of cancer cells, respectively. The parameters of the model that include four compartments of cells with different self-renewal and switching rates are obtained to validate the model throught experimental data. We showed that plasticity may increase or decrease the effect of imperfectness on the difference between fake and real proportions of positive cells. We also showed that plasticity may increase the difference of the *PD* of the cancer cells under different microenvironmental conditions.

It is clearly shown that by growing time, MFE of the cancer cells under hypoxic conditions becomes larger than the MFE for the cells under normoxic condition. We could show that by the time the probability of forming mammosphere increases, AMS decreases.

The imperfectness is considered initially to be a certain percentage of the population of cells, that we choose the single cells from in MFA. Increasing this imperfectness results in a cancer

cell population with higher probability of forming mammospheres even with bigger sizes. In addition, if in our stochastic analysis we use groups of few cells instead of single cell, we see the same effect on MFE and AMS.

Our theoretical analysis show that plasticity causes the cancer cells to form more mammospheres, and larger in size. We could also figure out the effect of plasticity on survival probability of positive cells using analytical stochastic modeling. It is shown that controlling the survival probability of positive cells is more effective by using the self-renewal rate of negative cells instead of positive cells.

Chapter 4

Experimental errors in cancer studies: sphere formation assay

Sphere formation assay (SFA) is a method of investigating the capacity of cancer cells to form colonies. In spite of a variety of studies using this assay, there is still not enough consistency in its application which is may be not required for the experimental analysis, but important in quantitative investigation. As a result, there are free parameters in the experiment, but these have not been explicitly discussed in the literature. Period of culturing and the initial cell number per well are two examples of the free parameters affecting the results including frequency of forming spheres and the size of the spheres. We show that without a standardized set of free parameters, it is difficult to establish conclusive results. The concept of inactive cores in spheres is also proposed, and the effects of this proposition are examined *in silico*.

4.1 Introduction

Sphere formation assay has been used in the last decade to present the capacity of the cancer stem cells in different cancer cell lines to form colonies. The spheres can be an aggregation of mammary gland cells, called mammospheres, or neural stem cells, called nuerospheres. The parameter of interest in this assay is the frequency of forming sphere, usually called sphere formation efficiency (SFE). Mammosphere formation efficiency (MFE) is the same parameter defined for mammary cells. Scientists have obtained MFE for different cancer cell lines such as breast and pancreatic cancer [41], [42]. They have examined the effect of epithelial to mesenchymal transition (EMT) [41], chemo- and radio- therapies [42], genetic regulations [43], and the microenvironment [35] on MFE. Neurosphere formation efficiency (NFE) can be also defined similarly for neural cells, which have been studied for the cancer cells under therapy and different microenvironments [7], [30]. Scientists have determined the potential of cancer cells to form spheres and how different kinds of stimulations affect this capacity using MFE and NFE.

In spite of several studies on SFA, the goal of the experiment is not about comparing the results with available experimental data of the same assay in the literature. Therefore, there is a lack

of consistency in the corresponding experimental procedure, which makes the quantitative analysis of experimental data incomparable. In its general application, usually 1000 or more wells, including a few separate cancer cell wells, are cultured and allowed to grow to form spheres for a period of time. By paying attention to the experiments, we can see important ambiguities in this procedure: 1) the number of cells in each well can be one or more; 2) the phenotypes of the cancer cells considered in the wells are not unique, as they can be CSCs or non-CSCs; 3) the time of culturing is not a predefined period. Therefore, the effects of variation of these free parameters on SFA should be examined to propose a universal methodology. The modification of SFA with due attention to the mentioned sources of errors may be helpful to provide a promising and conclusive comparison of the available results in the literature. Theoretical prediction is a useful tool to estimate the order of the errors caused by these ambiguities in SFA. Stochastic modeling has to be used in order to capture the behavior of cells in SFA. The two compartment model (TCM) seems to be a reliable model for this purpose and we use it in this chapter. In addition to the cancer stem cell hypothesis [2], [32] the existence of plasticity in the cancer cell population has been considered in this model. Therefore, the effects of phenotype on the SFA's results could be also captured using TCM.

4.2 Method

We use the two compartment model (TCM) to predict the behavior of cancer cells in SFA. In this model, the total population of cancer cells is considered to include two general phenotypes of CSCs and non-CSCs (Fig. 26). The divisions in this model include self-renewal and death of both phenotypes as well as switching between them.

On the basis of the definition of SFA, cancer cells are cultured in a medium for a few days. Some of the initial cancer cells form spheres (Fig. 26) that are considered to include CSCs and non-CSCs. Sphere formation assay should be modeled stochastically because of the low cell number limit. The stochastic behavior of the system is assumed to be Markovian. Therefore, equation (2.4) can be used to analyze the behavior of CSCs in SFAs. This equation can be solved numerically using Gillespie algorithm.

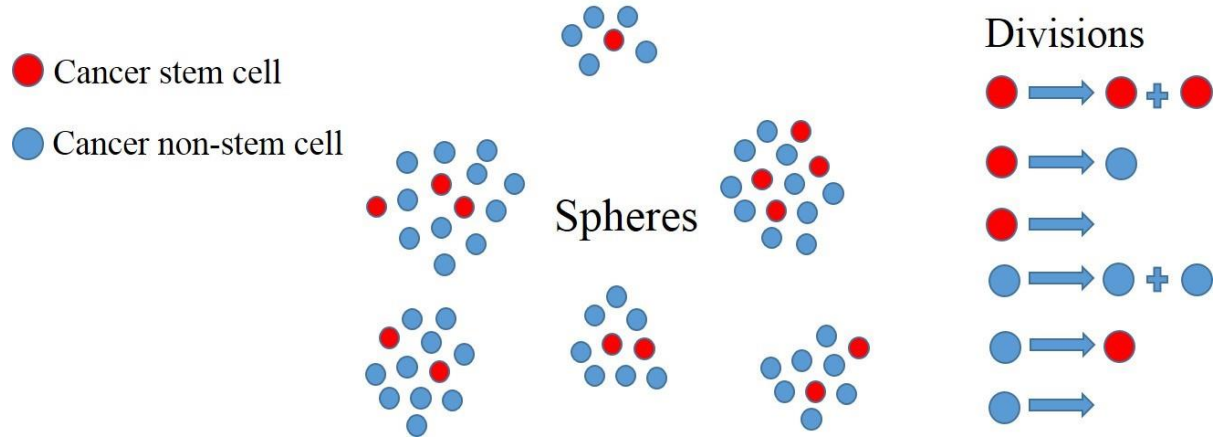

Figure 26 Schematic representation of spheres in SFA and the possible divisions hypothesized in TCM.

4.3 Results

Sphere formation assay has been employed during the last decade to investigate the colony formation capacity without a universality. The results of this assay can be used to judge the potential of initial cancer cells to form tumors. However, we need a universal methodology to compare the results of SFA for different cancer cell lines and under different microenvironmental conditions. The theoretical analysis prepared in this chapter is employed to clarify the artifacts of lacking a universal methodology for SFA. The experimental results of McCord et al., (2009) and Hjelmeland et al., (2011) are employed to show the possible errors. All of the results are obtained using TCM with the parameters validated by the experimental data of McCord et al., (2009) and Hjelmeland et al., (2011). It should be noted that both papers are dedicated to studying the glioma cells.

4.3.1 Period of experimentation

One of the important issues in SFA is the period of experimentation. In the usual procedure, the number of spheres formed in the culture medium are counted and reported after a period of time to show the potential of the considered cancer cells to form colonies under the assumed microenvironments, like normal, hypoxic or acidic. Most of the time, these spheres grow so that they reach together or reach the boundaries of the culture medium. Hence, the experiment

cannot be continued further and the formed spheres are reported as the frequency of forming spheres. We can see the large range of period of experimentation (4-14 days) in Table 11. If we can prepare the experimental conditions so that the cells reach their in-equilibrium state, they might form more spheres and the actual SFE might be larger.

Sphere formation efficiency is reported as a function of time in Fig. 27. The time variation of SFE in Fig. 27 reveals that an in-equilibrium value can be reached far beyond the 10 and 14 days used in the experiments of Hjelmeland et al., (2011) and McCord et al., (2009), respectively. It can be also seen that this steady state time is later in Fig. 27(b) (corresponding to the experimental result of McCord et al., (2009)). In addition, the variation of SFE with respect to time is different as can be seen in Fig. 25, where we can see that SFE changes faster between days 13 and 29 for the cancer cells under acidic and normal conditions, based on the results of Hjelmeland et al., (2011), than those validated by the results of McCord et al., (2009). As time passes, the difference of SFE between normal and acidic or normal and hypoxic conditions decreases. The dependency of this difference is so that, in the steady state condition, both normal and acidic conditions result in almost the same SFE (Fig. 27(a)).

The size of the sphere is another parameter showing the rate of growth of the colonies of cancer cells. We can determine the rate of tumor initiation from initial mutated cells using this parameter. This parameter can be also affected by changing the microenvironment. We show here that the time of measurement is very important (Fig. 28). It is shown in Fig. 28 that the difference of average sphere size (ASPS) in harsh and normal microenvironments grows over time. The difference grows exponentially so that, at the time stages in which the SFE saturates, the growth rate is much more than the difference in the initial time stages (Fig. 28). Hence, measuring the difference of ASPS in different microenvironments in initial time stages underestimates this difference at the time of saturation of SFE.

Table 11 Period of time the cells are cultured in SFA.

Reference	Final time of counting spheres
[44]	Day 4-7
[45]	Day 5
[46]	Day 5-7
[43]	Day 6
[47]	Day 7
[42]	Day 7
[48]	Day 7
[49]	Day 7
[7]	Day 10
[30]	Day 14

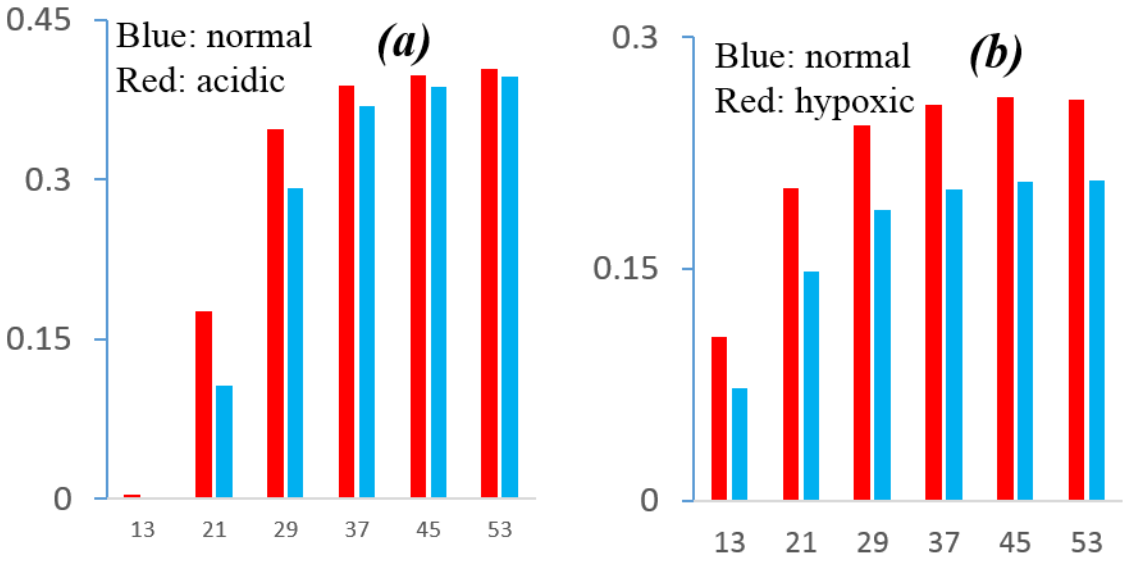

Figure 27 Variation of SFE with respect to time under different microenvironment obtained using TCM with the parameters validated by the experimental data of (a) Hjelmeland et al., (2011) and (b) McCord et al., (2009). (Start with 1000 CSCs.)

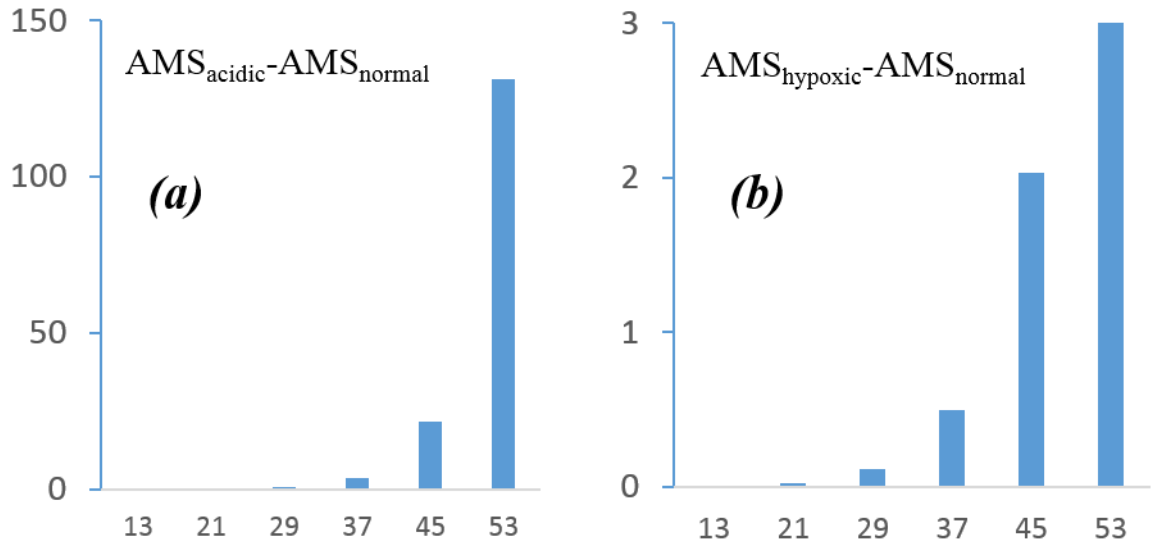

Figure 28 Variation of ASPS($\times 10^{-3}$) with respect to time under different microenvironment obtained using TCM with the parameters validated by the experimental data of (a) Hjelmeland et al., (2011) and (b) McCord et al., (2009). (Start with 1000 CSCs.)

4.3.2 Initial separate cells per well

In SFA, the experiments usually start with single cells. It means that for example 1000 separate single cells are in the culture medium and grow to form spheres. However, there are experiments with more than one cell in each well. For example, Hjelmeland et al., (2011) used 5 CSCs in each well.

We show that increasing the number of cells in each well results in higher SFE which goes toward a saturation point for 9 initial cells per well and more (Fig. 29). Figure 29 shows variation of SFE with respect to the number of positive cells in each well. The cells under both normal and acidic conditions, extension for the data of Hjelmeland et al., (2011), goes toward the same saturation point (Fig. 29(a)). It should be noted that the results using 5 cells per well is much greater than the results with one cell per well. The extended data of McCord et al., (2009) is also obtained (Fig. 29(b)) that shows even with 9 initial cell per well, there is still difference between SFE of the cancer cells under hypoxia versus normoxia.

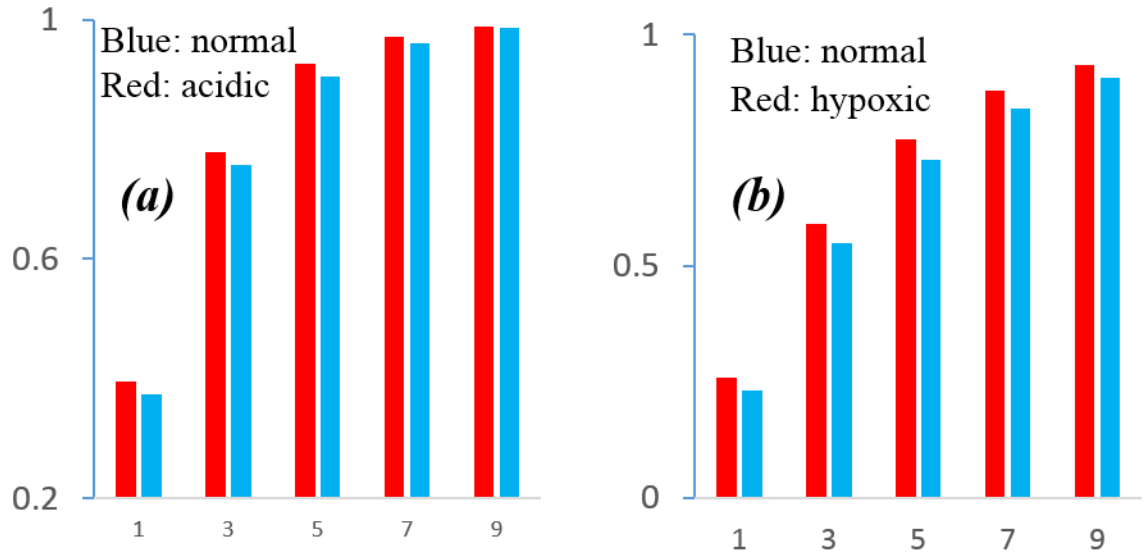

Figure 29 Dependency of SFE on the initial cells in each well. (Start with 1000 well of CSCs.)

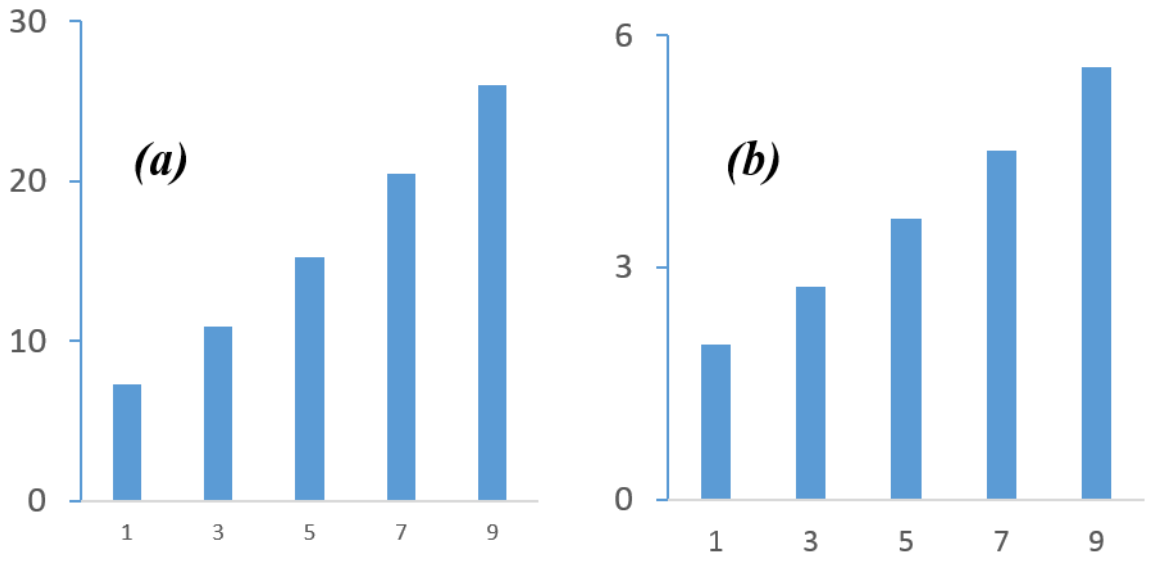

Figure 30 Dependency of ASPS on the initial cells in each well. (a) $ASPS_{acidic}$-$ASPS_{normal}$ and (b) $ASPS_{hypoxic}$-$ASPS_{normal}$(Start with 1000 well of CSCs.)

The dependency of the difference of ASS for the cells under harsh and normal conditions are also obtained (Fig. 30). The variation of both $ASPS_{acidic} - ASPS_{normal}$ and $ASPS_{hypoxic} -$

$ASPS_{normal}$ are almost linear with respect to the variation of the initial number of cells per well. The variation of $ASPS_{acidic} - ASPS_{normal}$ is much more than $ASPS_{hypoxic} - ASPS_{normal}$ in the considered range of initial cell number which is clear by comparison of Fig. 30(a) and (b).

4.3.3 Activity of cells

In the study of every colony of cancer cells there is an open question about their activity. Are all of them active? In the *in vivo* analysis, we usually consider a necrotic and quiescent inner regions in which the cells do not have the proliferative capacity. This inner region may exist also in the spheres when the cancer cells grow *in vitro*. We show that existence of this inner quiescent region has important effects on the results of SFA

We define the following relation for the active number of cells in the outer region of spheres by assuming the cancer cells have the average diameter of $10\ \mu m$.

$$N_{active} = Ceil\left(0.7\left(3(2.86N)^{2/3} - 6(2.86N)^{\frac{1}{3}} - 4\right)\right) \qquad \textbf{(4.1)}$$

where N is the total number of cells in each well. The coefficient *0.7* is applied because of existence of unoccupied space between the cells [34]. In this relation, we assume that the active cells are only the ones in the out layer of the sphere. Because the number of cells should be an integer number, the Ceil function is used in calculating the active number of cells.

The inactive cells exist in the middle of the spheres and their number increases with time. We show some of the differences caused by the existence of inner inactive region using the parameters obtained for the experimental results of McCord *et al*. (2009) (Figs. 31 and 32). Sphere formation efficiency of glioma stem cells under normal and hypoxic conditions are shown in Fig. 31. The obtained SFE for the spheres with inactive core is much less than the SFE for the spheres without inactive core. In normal condition (Fig. 31(a)), the SFE for the spheres with inactive core is almost negligible with respect to the SFE for the spheres without inactive core. Nevertheless, the variation of SFE with both assumptions, whether there is an inactive core or not, is similar. The effect of assuming an inactive core on ASPS is also shown

in Fig. 32. We can see that by assuming the inactive core in the spheres, ASPS is almost constant in the considered time range while it grows exponentially without this assumption. This constant value is less than the ASPS obtained for the spheres without the inactive core assumption through the considered time period.

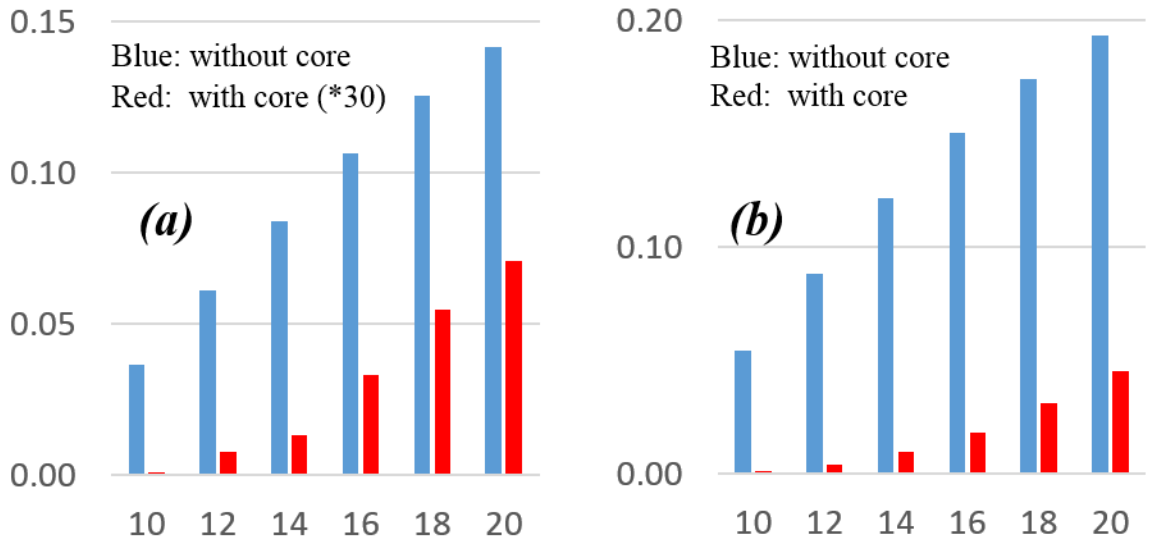

Figure 31 Variation of SFE with respect to time using TCM with the parameters validated by the experimental data of McCord et al., (2009) under (a) normal and (b) hypoxic conditions. (Start with 1000 single CSCs.)

4.4 Discussion

We showed that SFE and ASPS vary by changing the period of culturing (Figs. 27 and 28). There is a saturation for SFE which can be considered as the maximum sphere formation capacity of the cancer cells in every condition. To get the maximum capacity of cancer cells, we have to design the experiment so that the cells have enough time to grow and reach the saturation point.

Average sphere size increases exponentially with time. The variation of SFE and ASPS with respect to time in a different microenvironment clearly shows that comparing these parameters at different time stage of culturing could give us different results. It is possible that maximum

SFE, can be obtained with a longer period of culturing, is higher for some microenvironments with respect to others while in initial time stages, for example 10 days or less, it is lower.

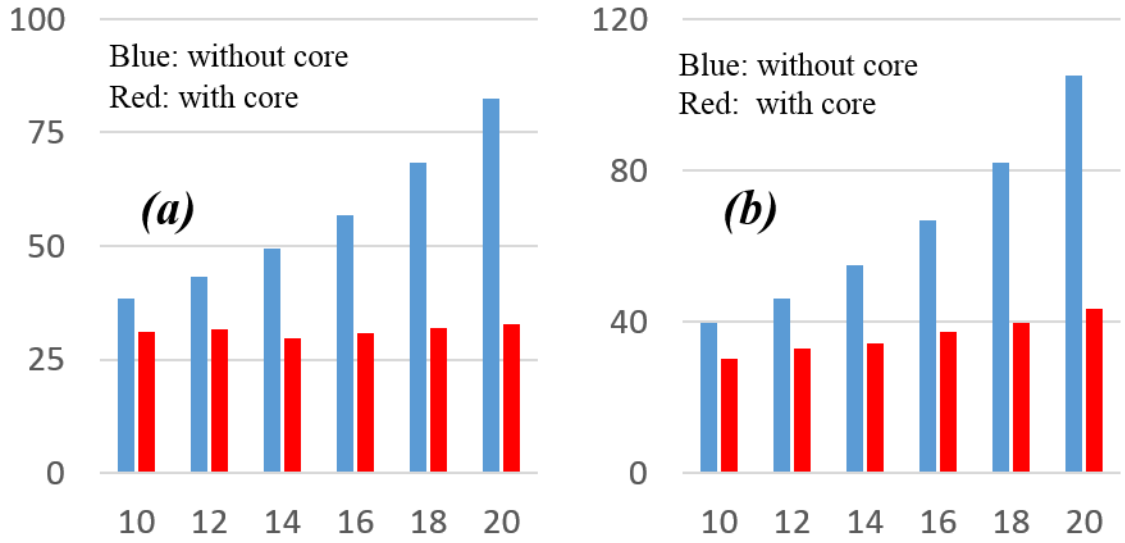

Figure 32 Variation of ASPS with respect to time using TCM with the parameters validated by the experimental data of McCord et al., (2009) under (a) normal and (b) hypoxic conditions. (Start with 1000 single CSCs.)

Another issue in SFA is the initial number of cancer cells in each well. Increasing the initial cells per well results in higher SFE toward reaching the full capacity that is 1. However, we can see that the difference of SFE under normal and acidic conditions decreases by increasing the initial number of cancer cells per well. Therefore, if we want to compare SFE under different microenvironments, the initial number of cells should be the same. Other than that, the comparison may not be meaningful. Average sphere size also depends on the initial number of cells per well and varies linearly with this number.

We also investigate the effect of existence of an inactive core through each sphere on the parameters of interest, SFE and ASPS, in SFA. If there is such a core, caused by dead or quiescent cells, both SFE and ASS will be less than the SFE and ASS we expect without this assumption (Figs. 31 and 32). This effect not only changes the values of these parameters such

as significant change of SFE in normal condition but also affects the dependency of ASPS with respect to time. Average sphere size is almost constant and the size of spheres do not grow by considering this assumption (Fig. 32).

We investigate the importance of time period of culturing, initial number of cells in each well and existence of inactive core on the results of sphere formation assay. We show the possible effects of these factors in this experiment. Experimental study is required following the theoretical analysis of this chapter to obtain a universal definition for SFA.

Chapter 5
Effect of phenotype switching on radiation therapy

In this chapter, two phenomenological models are employed to study the effects of phenotype switching on radiation therapy: the two-compartment model (TCM) and the proliferative-migratory model (PMCM). In the TCM, different ranges of self-renewal, death rates of positive and negative cells, and switching rates between these phenotypes are considered. The other model (PMCM) is also developed to investigate the effect of migration and switching between proliferative and migratory cancer cells on radiation therapy. Logistic growth of cancer cells is assumed in each model. The range of the parameters of both models is considered to satisfy certain biological criteria. We show that both total number of cells and proportion of positive cells, two important parameters after radiation therapy, are affected by changing different parameters such as plasticity and switching rate between proliferative and migratory phenotypes. More analysis has to be done and corresponding experimental and clinical investigation have to be designed properly to target phenotype switching as a method of increasing the efficiency of therapeutic procedures.

5.1 Introduction

Different phenotypes of cancer cells can migrate in the tumor. Increasing the migration capacity of cells increases the probability and rate of metastasis [41]. The epithelial to mesenchymal transition (EMT) is a process in which the cells in a tumor develop a high migratory capacity [41]. Mani *et al.* (2008) showed that Squamous cell carcinoma contains CSCs with two distinct phenotypes: 1) similar to normal epithelial cells and 2) migratory cells (formed by EMT). Two of the main causes of the tumor malignancy can be considered to be the growth of the CSC population and the migratory capacity of CSCs [50]. Similar to the theory of plasticity that shows dedifferentiation in cancer cell populations, migratory cells can be changed to form epithelial-like cells [50]. Transient expression of epithelial to mesenchymal transition-associated genes can be reversed by a mesenchymal to epithelial transition (MET), leading to epithelial dedifferentiation [50]. In addition to metastasis, increasing the population of migratory cancer cells in tumors affects the therapeutic procedures. Gene-expression

profiling showed upregulation of genes related to motility, and functional studies demonstrated that cell motility contributes to the invasive phenotype of malignant gliomas [51]. Glioma cells show a decreased proliferation rate and a relative resistance to apoptosis, which may contribute to chemotherapy and radiation therapy resistance [51]. The radioresistance-associated metastatic potential of cervical cancer cells has been also domonstrated experimentally [52]. Hence, we can say that metastasis often circumvents the efficacy of radiotherapy. On the other hand, radiotherapy can change the proportion of the migratory cell phenotype in the cancer cell population. In the absence of stimulation or inhibition, increasing doses of irradiation induced a dose-dependent enhancement of migrating cells [53]. Therefore, the effect of phenotype switching in radiation therapy and the reverse investigation can be useful to promote the efficiency of therapeutic procedures.

We study the effect of phenotype switching on radiation therapy using the phenomenological models. We employ these models to investigate the effects of phenotype switching on total numbers of cells and on the proportion of positive cells after hypo-fractionated and conventional radiotherapeutic protocols. This study tells us that control of phenotype switching, by chemotherapy, can be considered as a tool to reduce the final tumor size and recurrence probability.

5.2 Method

The two primary modes of medical interventions in treating cancer (apart from surgery) are chemotherapy and radiotherapy. Clinically, it is reported that over 50% of North American cancer patients undergo radiation therapy as part of their treatment regimen. Radiotherapy can be used either for palliative (i.e., to alleviate the pain) or curative (i.e., to eliminate the tumor) purposes. Several experimental studies have reported that a small population of cancer stem cells is responsible for unlimited growth of tumor, anti-cancer therapy resistance, and recurrence of a tumor. Additionally, the existence of different phenotypes with varied proliferation rates and radio (and/or chemo) sensitivities in the tumor population can have an impact on the treatment efficacy as well as on the recurrence of a tumor. Therefore, the dynamics of the cancer cell population during any therapeutic strategy is pivotal for

understanding tumor kinetics over time and designing an efficient treatment strategy to eliminate the tumor (and if possible decrease relapse). To investigate these effects, two mathematical models are used in this chapter that are based on the new theories of existence of cancer stem cell and plasticity in tumors. These mathematical frameworks include the TCM and an extension model to include proliferative-migratory mechanisms between cancer cells (Fig. 33).

Death rates in the models are assumed to be the cell killing rate of tumor cells by radiation. However, it can be caused by different external or internal stimulation in general. To have a more realistic prediction, the death rates (or killing rates) are considered to be pulsatile. Radiotherapy is given as a step function as 10 minutes per fraction (i.e., dose of *d* Gy per day). From the modeling perspective, the cell killing term due to radiation is assumed to be non-zero only during 10 minutes of radiation administered every day (otherwise, it is assumed to be zero).

The population of the positive and negative cells can be dynamically modeled using the following ordinary differential equations that are driven using the TCM

$$\begin{aligned} \frac{dS}{dt} &= \rho_{ss}\left(1-\frac{S+P}{K}\right)S - \rho_{sp}S + \rho_{ps}P - \Gamma_s S \\ \frac{dP}{dt} &= \rho_{pp}\left(1-\frac{S+P}{K}\right)P - \rho_{ps}P + \rho_{sp}S - \Gamma_p P \end{aligned} \qquad \textbf{(5.1)}$$

where *S* and *P* represent number of positive and negative cells, respectively. The parameters of the TCM are briefly described in Table 12. Except the logistic self-renewal of both positive and negative cell populations, other terms in Eq. (5.1) including the switching and death of the phenotypes are considered to be linear.

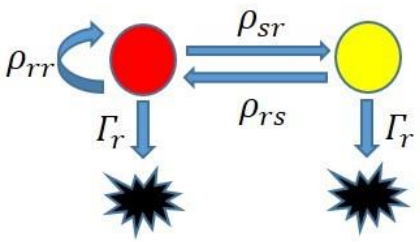

Figure 33 Schematic representation of proliferative-migratory cell model (PMCM).

5.2.1 Proliferative-migratory cell model (PMCM)

We can consider the tumor cells as proliferative and migratory phenotypes in general (Fig. 33). In this framework, we do not consider the difference between the characteristics of the cells these phenotypes. In addition, we neglect the proliferative capacity of the migratory phenotype.

In some tumors, experimental studies support the existence of both proliferative phenotype (with zero or non-zero migration) and migratory phenotype (with zero or non-zero proliferation) [41]. In this model, we assume that proliferative cells have self-renewing potential, while migratory cells can just switch to proliferative ones. Similar to the TCM, the death rates are also considered for both populations of cells which are active only during radiation and are neglected under normal conditions (i.e., during non-irradiation time). These assumptions help us to study the effect of switching between proliferative and migratory phenotypes on the radio-resistance of the tumor and also on its probability of recurrence.

The following ODEs can be written for the time dependent population of proliferative and migratory cells.

$$\begin{aligned} \frac{dR}{dt} &= \rho_{rr}\left(1-\frac{R+M}{K}\right)R-\rho_{rm}R+\rho_{mr}M-\Gamma_r R \\ \frac{dM}{dt} &= \rho_{rm}R-\rho_{mr}M-\Gamma_m M \end{aligned} \qquad \textbf{(5.2)}$$

where *M* and *R* represent the population of migratory and proliferative cells, respectively. The parameters of this model are also presented in Table 12.

5.3 Results

The purpose of cancer treatments is to ideally eliminate the cancerous cells completely or reduce the number of cancer cells to a larger extent. Tumor recurrence is another issue in the therapeutic procedures of cancer patients. On the basis of the cancer stem cell hypothesis [2], [32], more cancer stem cells after treatment results in a higher chance of recurrence. Therefore, these two parameters are studied using TCM and PMCM.

Table 12 Definition of the parameters used in the TCM and PMCM.

Two compartment model	
ρ_{ss}	Self-renewal rate of positive cells
ρ_{sp}	Differentiation rate
ρ_{ps}	Dedifferentiation rate
ρ_{pp}	Self-renewal rate of negative cells
Γ_s	Death rate of positive cells
Γ_p	Death rate of negative cells
N	Total number of cells
K	Maximum number of cells
Proliferative-migratory cell model	
ρ_{rr}	Self-renewal of proliferative cells
ρ_{rm}	Rate of switching to migratory phenotype
ρ_{mr}	Rate of switching to proliferative phenotype
Γ_r	Death rate of proliferative cells

5.3.1 Two compartment model

It has been shown that there should be a dedifferentiation or plasticity in the population of cancer cells that enables negative cells to produce positive ones [10], [40]. Hence, it has been also proposed that plasticity can be an important factor to determine aggressiveness of tumors [40]. We include this factor in the TCM to investigate its importance in the efficacy of the treatment strategies. Another factor that directly affects the efficiency of treatment is the killing rate of each phenotype, positive and negative cells. Negative cells are more sensitive to radiation therapy or other treatments, based on the assumptions in the cancer stem cell hypothesis [2], [32]. The death rates of the phenotypes are considered to be non-zero during the time of treatment. By considering death rate of positive cells to be equal to *1* per day, variable Γ_p/Γ_s shows the killing rate of the negative phenotype.

In order to study the effect of radiation therapy, we use two protocols: hypo-fractionated radiotherapy and conventional radiotherapy. Total dosage is the same in both procedures. In hypo-fractionated radiotherapy, *3* Gray is applied in *20* days while in conventional radiotherapy 2 Gray is applied in *30* days. The death rates during radiation can be calculated as follows for each treatment strategy [35].

$$\text{Death rate} = \alpha(\text{Dose per day})/\tau \qquad \textbf{(5.3)}$$

where $\alpha = 18$ and $\tau = 15$ min.

The variation of the total number of cells after two types of radiotherapies, conventional and hypo-fractionation, are shown with respect to the dedifferentiation rate in Fig. 34. It is obvious that dedifferentiation decreases the effect of therapy. Hence, the final population of cancer cells is bigger in the colonies with higher degree of dedifferentiation. This effect is different for the two types of regimens; the population of cancer cells is smaller after hypo-fractionated radiotherapy. Different values of Γ_p/Γ_s are considered in Fig. 34 which clarifies the importance of this ratio. The total number of cancer cells is obviously less for higher values of this fraction.

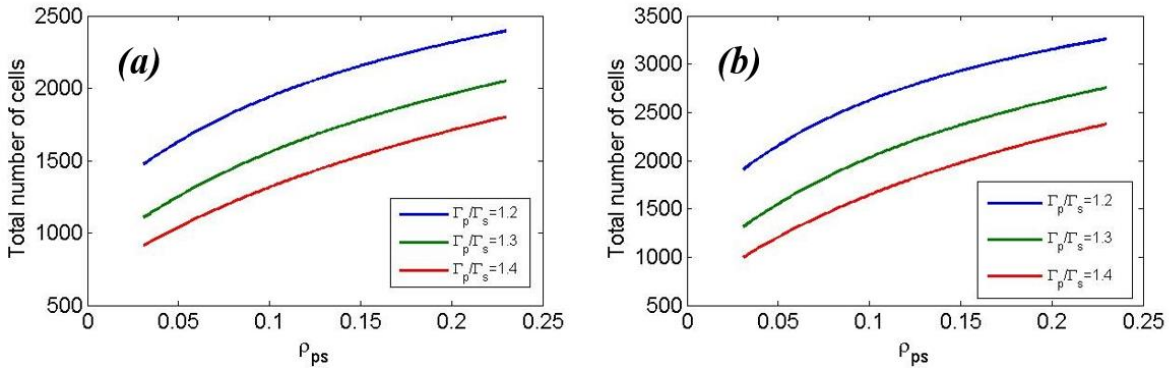

Figure 34 Total number of cells versus dedifferentiation rate for different Γ_p/Γ_s after (a) hypo-fractionated radiotherapy and (b) conventional radiotherapy.

Because of the self-renewal capacity of cancer stem cells, recurrence of a tumor depends on the proportion of positive cells that are left over at the end of the treatment. Hence, more positive cells in the system corresponds to a higher chance of recurrence.

The dependency of the proportion of positive cells on plasticity is illustrated in Fig. 35 for both hypo-fractionated and conventional regimens. The behavior of cancer cell populations for both protocols is almost identical as shown in this figure. Increasing the plasticity increases the proportion of positive cells. This result can be also intuitively understood; higher values of plasticity increases the population of positive cells, and decreases the negative cancer cell population. Therefore, the chance of tumor recurrence is higher for the cancer cell populations associated with higher plasticity.

It has been shown in recent studies that microenvironment is an important factor that changes plasticity in cancer cell populations [5]. Hypoxic conditions, or lower oxygen concentrations, increase plasticity in tumors. In hypoxia, the effect of radiotherapy is minimal and cancer cells that are left over after treatment are increased. Therefore, one of the possible reasons for radioresistance in the hypoxic region of the tumor may be due to plasticity. However, several biological studies are required to validate this fact. Additionally, the fraction of positive cells under hypoxic conditions with higher plasticity is elevated, which may be one of the reasons for tumor recurrence.

We showed that the ratio of death rate of negative cells to positive cells is another important factor in the TCM. Dependency of number of cancer cells after radiotherapy on Γ_p/Γ_s is shown in Fig. 36. As death rate of negative cells increases, total number of cells decreases. Interestingly, the effect of plasticity on this trend is different. Near the minimum value of the death rate $\Gamma_p/\Gamma_s = 1$, the number of cells is higher for lower plasticity. The cell number becomes higher for the higher negative cell death rate. It is based on the fact that the dependency of the number of cancer cells on Γ_p/Γ_s is increased by decreasing plasticity. In other words, for lower dedifferentiation rates, the dependency of tumor size on the death rate of negative cells increases.

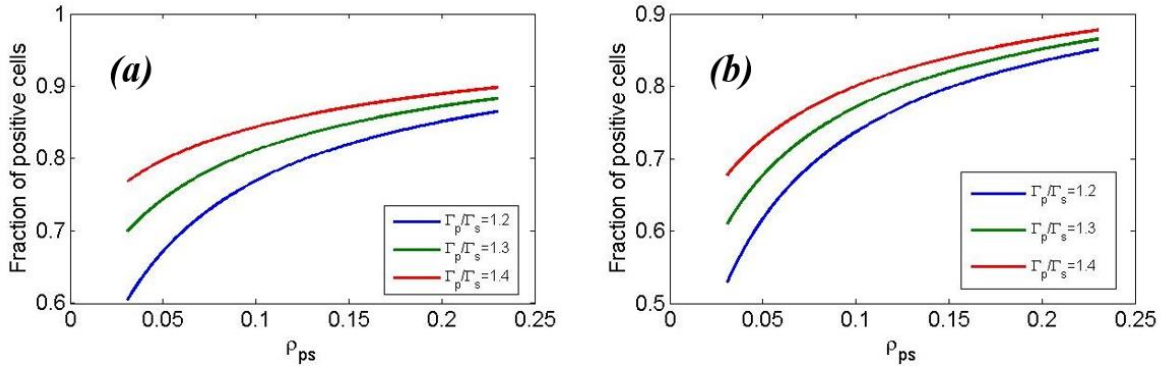

Figure 35 Proportion of positive cells versus dedifferentiation rate for different Γ_p/Γ_s after (a) hypo-fractionated and (b) conventional radiotherapy.

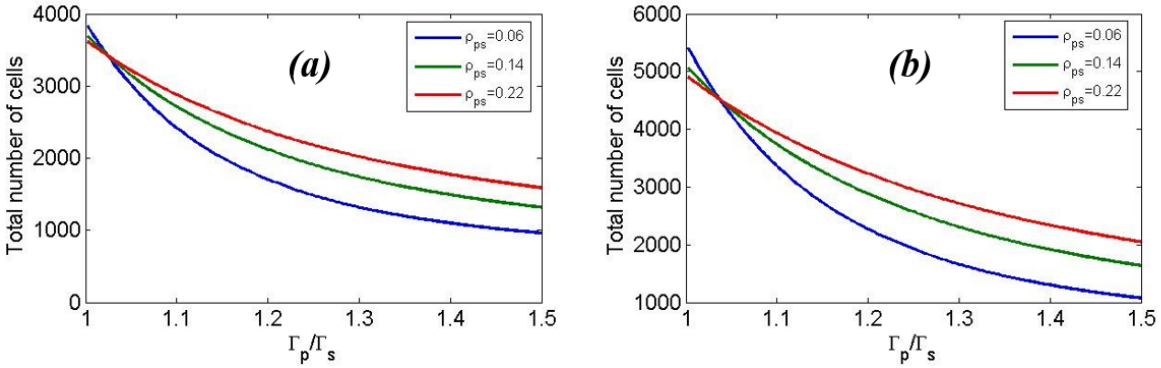

Figure 36 Total number of cells versus Γ_p/Γ_s for different dedifferentiation rate after (a) hypo-fractionated and (b) conventional radiotherapy.

The effect of the death rate of negative cells on proportion of positive cells is also studied (Fig. 37). Increasing the death rate of negative cells reduces the population of this phenotype in the system which results in higher proportions of positive cells. A higher fraction of positive cells leads to an increase in tumor recurrence. Therefore, an efficient treatment strategy should be designed with due attention to the effect of death rate of negative cells on increasing the probability of recurrence.

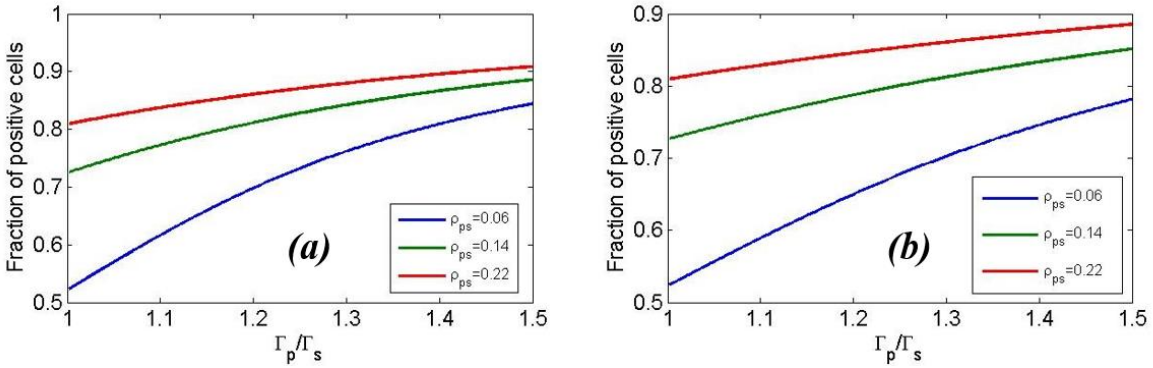

Figure 37 Proportion of positive cells versus Γ_p/Γ_s for different dedifferentiation rate after (a) hypo-fractionated radiotherapy and (b) conventional radiotherapy.

5.3.2 Proliferative-migratory cell model (PMCM)

The positive and negative phenotypes in TCM can be assumed to be a total population of proliferative cancer cells. On the basis of this assumption, total tumor cells can be considered to be proliferative or migratory that is the assumption of the PMCM.

Two important free parameters are chosen in this model to investigate the behavior of tumor cells during and after radiotherapy including rate of switching ρ_{mr} and ratio of migratory cell death rate to proliferative cell death rate Γ_m/Γ_r.

The effects of increasing migratory cell death rate on both protocols, hypo-fractionated and conventional, are shown in Fig. 38. Increasing death rate of each phenotype in tumor obviously decreases the final number of cells. However, this trend depends on various parameters such as migratory-proliferative switching rate ρ_{mr} (which is our concern in this framework). Although the number of cancer cells after treatment is less for a lower switching rate, dependency of tumor size, e.g., total number of cancer cells, on the death rate of migratory phenotype decreases. Therefore, this switching rate affects the efficiency of the treatment.

In addition to the effect of death rate of migratory phenotype on tumor size, it also affects the recurrence risk by changing the proportion of proliferative cells (Fig. 39). The proportion of proliferative cells linearly increases as the value of Γ_m/Γ_r increases (Fig. 39). Switching rate

between phenotypes also are important effect on the proportion of proliferative cells in the system. As shown in Fig. 39, increasing switching rate causes higher proportion of proliferative cells as well as a higher dependency of this fraction on Γ_m/Γ_r.

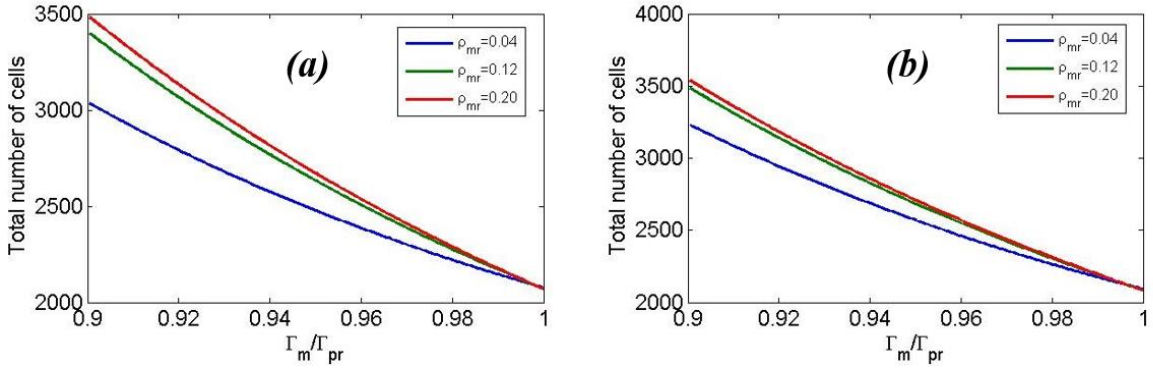

Figure 38 Total number of cells versus Γ_m/Γ_r for different switching rates ρ_{mr} after (a) hypo-fractionated radiotherapy and (b) conventional radiotherapy.

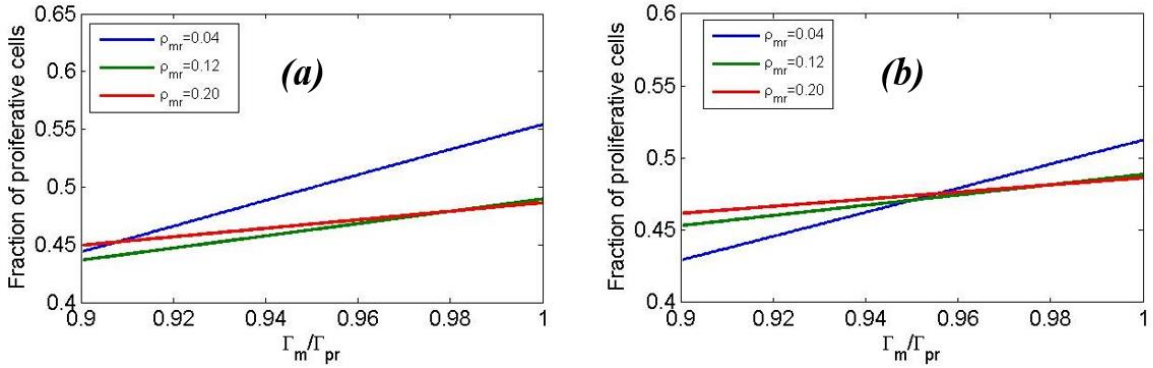

Figure 39 Proportion of positive cells versus Γ_m/Γ_r for different switching rates ρ_{mr} after (a) hypo-fractionated radiotherapy and (b) conventional radiotherapy.

It was shown that switching between migratory and proliferative compartment is an important factor in cancer cell growth and its treatment [41]. The total number of cancer cells and the proportion of proliferative cancer cells versus ρ_{mr}, after radiotherapy, are shown in Figs. 40 and 41. It should be noted that the variations for various death ratios Γ_m/Γ_r are identical. Increase in tumor size by increasing switching rate is clearly shown in Fig. 40. It is considered that during treatment the switching rate from migratory to proliferative population is

negligible, i.e., equal to zero, but the switching between proliferative to migratory phenotype is assumed to be enhanced significantly during irradiation. By increasing switching rate, the cancer cells go from the proliferative compartment with greater death rate to the migratory compartment with smaller death rates. Therefore, the total killing rate decreases and the total population of cancer cells will be greater after treatment.

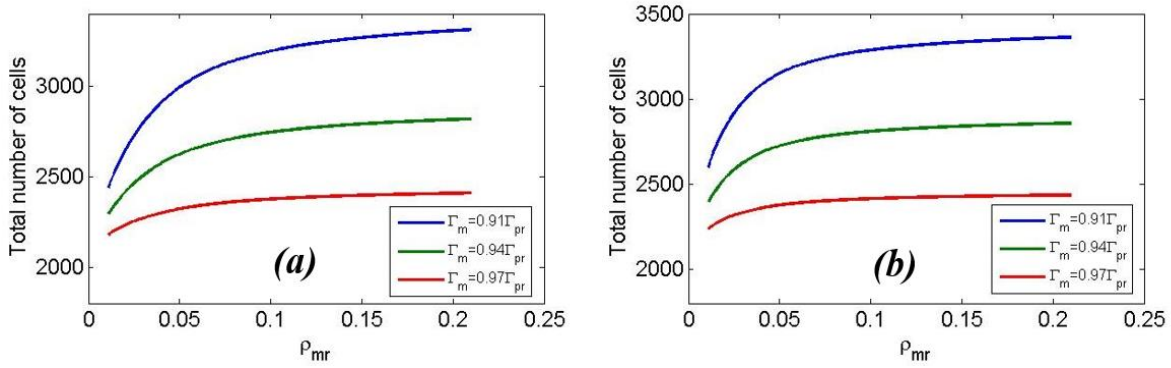

Figure 40 Total number of cells versus ρ_{mr} for different Γ_m/Γ_r after (a) hypo-fractionated radiotherapy and (b) conventional radiotherapy.

The switching rate clearly changes the fraction of proliferative cells, as shown in Fig. 41. Increasing switching rate is equal to decreasing proliferative cells and consequently increasing migratory cells. However, it seems that there is a saturation so that for values greater than $\rho_{mr} \approx 0.15$ this rate does not have any significant effect on the proportion of positive cells (Fig. 41). This behavior can be also seen in Fig. 40 for the total number of cancer cells at the end of the treatment.

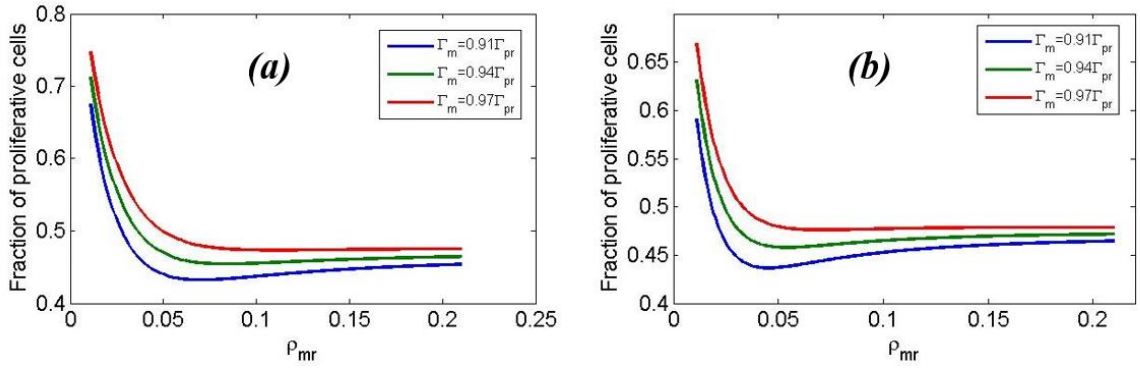

Figure 41 Proportion of positive cells versus ρ_{mr} for different Γ_m/Γ_r after (a) hypo-fractionated radiotherapy and (b) conventional radiotherapy.

5.4 Discussion

Two-compartment model is used to show the effect of switching between positive and negative phenotypes in cancer cell populations. Increasing plasticity results in a larger tumor and a higher proportion of positive cells after treatments. Therefore, the efficiency of radiation therapy decreases by increasing the plasticity and controlling this parameter can effectively increase the efficiency of the therapeutic procedures. In addition, we can decrease the probability of tumor recurrence and its growth rate by controlling plasticity in tumors.

Increasing Γ_p/Γ_s(representing the relative death rate of negative cells) decreases the total number of cells while increasing the proportion of positive cells after radiation therapy. It can be deduced from the model without calculation that a higher death rate of negative cells results in a higher proportion of positive cells. It also decreases the total number of the cells because of the higher death rate of one phenotype of the population.

The death rate proportion Γ_m/Γ_r and switching rate ρ_{mr} are also used as two free parameters in the PMCM to investigate the behavior of migratory cells in the cancer cell population. The total number of cells decreases while the fraction of proliferative cells increases by increasing Γ_m/Γ_r. A lower proportion of migratory cells obtained with higher Γ_m/Γ_r results in the higher efficiency of radiation therapy [52]. The self-renewal rate of migratory cells are considered to be negligible. Hence, augmentation of ρ_{mr} enhances the number of cancer cells and reduces

the proportion of proliferative cells. Both of these effects reduce the efficiency of radiotherapy and result in a higher number of cancer cells and proportion of migratory cells after treatment. Therefore, controlling the switching rate between migratory and proliferative phenotypes may have a significant impact on the efficiency of radiotherapy.

Chapter 6
Conclusion and contributions

We showed in this thesis that both stochastic and deterministic behavior of cancer cells should be taken into consideration to properly fit the model parameters in CSC studies. The developed models can be used to estimate the behavior of cancer cells under different microenvironments as well as for different therapeutic procedures. The models may also help in modifying the experimental procedures.

All of the presented models are temporal and the spatio-temporal growth of the cells is not taken into consideration. Hence, the models can be extended to include spatial variables to capture the invasion, migration or other spatial biological parameters involved in tumor growth *in vitro* and *in vivo.*

In addition to the projects presented in the previous chapters, I have contributed to two other projects. In collaboration with Dr. Mani's group, MD Anderson Cancer Centre, the TCM was used in to capture the behavior of breast cancer cells under hypoxia. Hypoxia, or oxygen deficiency, is known to be associated with breast tumor progression, resistance to conventional therapies and poor clinical prognosis. Highly proliferative tumors often outgrow their blood supply resulting in a necrotic core surrounded by a hypoxic region, underscoring the importance of understanding the clinical relevance of hypoxia and its role in tumor progression. In this work, we examined the impact of hypoxia on EMT-associated cancer stem cell (CSC) properties, by culturing transformed human mammary epithelial cells under normoxic and hypoxic conditions, and applying in silico mathematical modeling to simulate the impact of hypoxia on the acquisition of CSC attributes and the transitions between differentiated and stem-like states. Our results indicated that both the heterogeneity and the plasticity of the transformed cell population are enhanced by exposure to hypoxia, resulting in a shift towards a more stem-like population with increased EMT features.

I was also involved in a project on the synergetic behavior between intracellular antioxidant families using kinetic equations for the relevant chemical reaction. We know that glutathione

peroxidase (GPx), peroxiredoxin (Prx), and catalase are the major antioxidants at the cellular level and protecting cell compartments against hydrogen peroxide (H_2O_2). In addition, they affect cellular processes such as cell signaling by modulating H_2O_2. In this project, we demonstrated that there is a synergetic coupling between GPxs, Prxs themselves and also with other antioxidants when the GPxs and Prxs are not in their saturated reduced form. This is due to a change in the activity of glutathione peroxidases and peroxiredoxins as a result of a change in the concentrations of other antioxidants. We used a perturbative method to analytically calculate the concentration of H_2O_2 as a functions of the production rate of H_2O_2 and the concentration of various antioxidants in a quasi-steady state. This derivation shows clearly that why antioxidants behaves in a correlated manner and why any change in the activity of one of them translates to a change in the activity of other antioxidants. Our results showed that an increase in the activity of GPxs or Prxs might not be due to a genetic switch but that could be the result of increase in the activity of other antioxidants.

Bibliography

[1] D. Hanahan and R. A. Weinberg, “Hallmarks of cancer: the next generation.,” *Cell*, vol. 144, no. 5, pp. 646–74, Mar. 2011.

[2] D. Bonnet and J. E. Dick, “Human acute myeloid leukemia is organized as a hierarchy that originates from a primitive hematopoietic cell,” *Nat. Med.*, vol. 3, no. 7, pp. 730–737, Jul. 1997.

[3] P. B. Gupta, C. L. Chaffer, and R. A. Weinberg, “Cancer stem cells: mirage or reality?,” *Nat. Med.*, vol. 15, no. 9, pp. 1010–2, Sep. 2009.

[4] J. E. Moulder and S. Rockwell, “Tumor hypoxia: its impact on cancer therapy,” *Cancer Metastasis Rev.*, vol. 5, no. 4, pp. 313–341, 1987.

[5] T. van den Beucken, E. Koch, K. Chu, R. Rupaimoole, P. Prickaerts, M. Adriaens, J. W. Voncken, A. L. Harris, F. M. Buffa, S. Haider, M. H. W. Starmans, C. Q. Yao, M. Ivan, C. Ivan, C. V Pecot, P. C. Boutros, A. K. Sood, M. Koritzinsky, and B. G. Wouters, “Hypoxia promotes stem cell phenotypes and poor prognosis through epigenetic regulation of DICER.,” *Nat. Commun.*, vol. 5, p. 5203, Jan. 2014.

[6] J. M. Heddleston, Z. Li, J. D. Lathia, S. Bao, A. B. Hjelmeland, and J. N. Rich, “Hypoxia inducible factors in cancer stem cells.,” *Br. J. Cancer*, vol. 102, no. 5, pp. 789–95, Mar. 2010.

[7] A. B. Hjelmeland, Q. Wu, J. M. Heddleston, G. S. Choudhary, J. MacSwords, J. D. Lathia, R. McLendon, D. Lindner, A. Sloan, and J. N. Rich, “Acidic stress promotes a glioma stem cell phenotype.,” *Cell Death Differ.*, vol. 18, no. 5, pp. 829–40, May 2011.

[8] S. Zapperi and C. A. M. La Porta, “Do cancer cells undergo phenotypic switching? The case for imperfect cancer stem cell markers.,” *Sci. Rep.*, vol. 2, p. 441, Jan. 2012.

[9] P. B. Gupta, C. M. Fillmore, G. Jiang, S. D. Shapira, K. Tao, C. Kuperwasser, and E. S. Lander, “Stochastic state transitions give rise to phenotypic equilibrium in populations of cancer cells.,” *Cell*, vol. 146, no. 4, pp. 633–44, Aug. 2011.

[10] C. L. Chaffer, I. Brueckmann, C. Scheel, A. J. Kaestli, P. A. Wiggins, L. O. Rodrigues, M. Brooks, F. Reinhardt, Y. Su, K. Polyak, L. M. Arendt, C. Kuperwasser, B. Bierie, and R. A. Weinberg, “Normal and neoplastic nonstem cells can spontaneously convert to a stem-like state.,” *Proc. Natl. Acad. Sci. U. S. A.*, vol. 108, no. 19, pp. 7950–5, May 2011.

[11] N. D. Marjanovic, R. A. Weinberg, and C. L. Chaffer, “Cell plasticity and heterogeneity in cancer.,” *Clin. Chem.*, vol. 59, no. 1, pp. 168–79, Jan. 2013.

[12] T. Reya, S. J. Morrison, M. F. Clarke, and I. L. Weissman, “Stem cells, cancer, and cancer stem cells.,” *Nature*, vol. 414, no. 6859, pp. 105–11, Nov. 2001.

[13] P. Dalerba and M. F. Clarke, “Cancer stem cells and tumor metastasis: first steps into uncharted territory.,” *Cell Stem Cell*, vol. 1, no. 3, pp. 241–2, Sep. 2007.

[14] J. E. Visvader and G. J. Lindeman, “Cancer stem cells in solid tumours: accumulating evidence and unresolved questions.,” *Nat. Rev. Cancer*, vol. 8, no. 10, pp. 755–68, Oct. 2008.

[15] P. B. Dirks, “Brain tumor stem cells: bringing order to the chaos of brain cancer.,” *J. Clin. Oncol.*, vol. 26, no. 17, pp. 2916–24, Jun. 2008.

[16] C. Venugopal, N. Li, X. Wang, B. Manoranjan, C. Hawkins, T. Gunnarsson, R. Hollenberg, P. Klurfan, N. Murty, J. Kwiecien, F. Farrokhyar, J. P. Provias, C. Wynder, and S. K. Singh, “Bmi1 marks intermediate precursors during differentiation of human brain tumor initiating cells.,” *Stem Cell Res.*, vol. 8, no. 2, pp. 141–53, Mar. 2012.

[17] B. G. Hollier, K. Evans, and S. A. Mani, “The epithelial-to-mesenchymal transition and cancer stem cells: a coalition against cancer therapies.,” *J. Mammary Gland Biol. Neoplasia*, vol. 14, no. 1, pp. 29–43, Mar. 2009.

[18] A. Eramo, F. Lotti, G. Sette, E. Pilozzi, M. Biffoni, A. Di Virgilio, C. Conticello, L. Ruco, C. Peschle, and R. De Maria, “Identification and expansion of the tumorigenic lung cancer stem cell population.,” *Cell Death Differ.*, vol. 15, no. 3, pp. 504–14, Mar. 2008.

[19] C. Lagadec, E. Vlashi, L. Della Donna, Y. Meng, C. Dekmezian, K. Kim, and F. Pajonk, “Survival and self-renewing capacity of breast cancer initiating cells during fractionated radiation treatment.,” *Breast Cancer Res.*, vol. 12, no. 1, p. R13, Jan. 2010.

[20] F. Michor, T. P. Hughes, Y. Iwasa, S. Branford, N. P. Shah, C. L. Sawyers, and M. A. Nowak, “Dynamics of chronic myeloid leukaemia.,” *Nature*, vol. 435, no. 7046, pp. 1267–70, Jun. 2005.

[21] R. Ganguly and I. K. Puri, “Mathematical model for the cancer stem cell hypothesis.,” *Cell Prolif.*, vol. 39, no. 1, pp. 3–14, Feb. 2006.

[22] R. V Solé, C. Rodríguez-Caso, T. S. Deisboeck, and J. Saldaña, “Cancer stem cells as the engine of unstable tumor progression.,” *J. Theor. Biol.*, vol. 253, no. 4, pp. 629–37, Aug. 2008.

[23] A. Paguirigan, D. J. Beebe, B. Liu, and C. Alexander, “Mammary stem and progenitor cells: tumour precursors?,” *Eur. J. Cancer*, vol. 42, no. 9, pp. 1225–36, Jun. 2006.

[24] A. Paguirigan, D. J. Beebe, and C. M. Alexander, “Simulating mouse mammary gland development: cell ageing and its relation to stem and progenitor activity.,” *Cell Prolif.*, vol. 40, no. 1, pp. 106–24, Feb. 2007.

[25] H. Enderling, A. R. A. Anderson, M. A. J. Chaplain, A. Beheshti, L. Hlatky, and P. Hahnfeldt, “Paradoxical dependencies of tumor dormancy and progression on basic cell kinetics.,” *Cancer Res.*, vol. 69, no. 22, pp. 8814–21, Nov. 2009.

[26] C. Turner and M. Kohandel, “Quantitative approaches to cancer stem cells and epithelial-mesenchymal transition.,” *Semin. Cancer Biol.*, vol. 22, no. 5–6, pp. 374–8, Oct. 2012.

[27] C. Turner and M. Kohandel, “Investigating the link between epithelial-mesenchymal transition and the cancer stem cell phenotype: A mathematical approach.,” *J. Theor. Biol.*, vol. 265, no. 3, pp. 329–35, Aug. 2010.

[28] “Cancer Stem Cells — NEJM.” [Online]. Available: http://www.nejm.org/doi/full/10.1056/NEJMra061808. [Accessed: 18-Feb-2015].

[29] C. A. M. La Porta, S. Zapperi, and J. P. Sethna, “Senescent cells in growing tumors: population dynamics and cancer stem cells.,” *PLoS Comput. Biol.*, vol. 8, no. 1, p. e1002316, Jan. 2012.

[30] A. M. McCord, M. Jamal, U. T. Shankavaram, U. T. Shankavarum, F. F. Lang, K. Camphausen, and P. J. Tofilon, “Physiologic oxygen concentration enhances the stem-like properties of CD133+ human glioblastoma cells in vitro.,” *Mol. Cancer Res.*, vol. 7, no. 4, pp. 489–97, Apr. 2009.

[31] D. T. Gillespie, “Exact stochastic simulation of coupled chemical reactions,” *J. Phys. Chem.*, vol. 81, no. 25, pp. 2340–2361, Dec. 1977.

[32] T. Lapidot, C. Sirard, J. Vormoor, B. Murdoch, T. Hoang, J. Caceres-Cortes, M. Minden, B. Paterson, M. A. Caligiuri, and J. E. Dick, “A cell initiating human acute myeloid leukaemia after transplantation into SCID mice.,” *Nature*, vol. 367, no. 6464, pp. 645–8, Feb. 1994.

[33] R. K. Sachs, W. F. Heidenreich, and D. J. Brenner, “Dose timing in tumor radiotherapy: Considerations of cell number stochasticity,” *Math. Biosci.*, vol. 138, no. 2, pp. 131–146, Dec. 1996.

[34] C. Turner, “Mathematical Modelling of Cancer Stem Cells.” 06-Aug-2009.

[35] A. Dhawan, K. Kaveh, M. Kohandel, and S. Sivaloganathan, “Stochastic model for tumor control probability: effects of cell cycle and (a)symmetric proliferation.,” *Theor. Biol. Med. Model.*, vol. 11, no. 1, p. 49, Jan. 2014.

[36] C. Phipps and M. Kohandel, “Mathematical model of the effect of interstitial fluid pressure on angiogenic behavior in solid tumors,” *Comput. Math. Methods Med.*, vol. 2011, 2011.

[37] S. Bao, Q. Wu, S. Sathornsumetee, Y. Hao, Z. Li, A. B. Hjelmeland, Q. Shi, R. E. McLendon, D. D. Bigner, and J. N. Rich, “Stem cell-like glioma cells promote tumor angiogenesis through vascular endothelial growth factor.,” *Cancer Res.*, vol. 66, no. 16, pp. 7843–8, Aug. 2006.

[38] J. L. Harris, M. Stocum, L. Roberts, C. Jiang, J. Lin, and K. Sprott, “Quest for the Ideal Cancer Biomarker: An Update on Progress in Capture and Characterization of Circulating Tumor Cells,” *Drug Dev. Res.*, vol. 74, no. 2, pp. 138–147, Mar. 2013.

[39] R. Gunawan, Y. Cao, L. Petzold, and F. J. Doyle, "Sensitivity analysis of discrete stochastic systems.," *Biophys. J.*, vol. 88, no. 4, pp. 2530–40, Apr. 2005.

[40] C. L. Chaffer, N. D. Marjanovic, T. Lee, G. Bell, C. G. Kleer, F. Reinhardt, A. C. D'Alessio, R. A. Young, and R. A. Weinberg, "Poised chromatin at the ZEB1 promoter enables breast cancer cell plasticity and enhances tumorigenicity.," *Cell*, vol. 154, no. 1, pp. 61–74, Jul. 2013.

[41] S. A. Mani, W. Guo, M.-J. Liao, E. N. Eaton, A. Ayyanan, A. Y. Zhou, M. Brooks, F. Reinhard, C. C. Zhang, M. Shipitsin, L. L. Campbell, K. Polyak, C. Brisken, J. Yang, and R. A. Weinberg, "The epithelial-mesenchymal transition generates cells with properties of stem cells.," *Cell*, vol. 133, no. 4, pp. 704–15, May 2008.

[42] E. Lonardo, M. Cioffi, P. Sancho, Y. Sanchez-Ripoll, S. M. Trabulo, J. Dorado, A. Balic, M. Hidalgo, and C. Heeschen, "Metformin targets the metabolic achilles heel of human pancreatic cancer stem cells.," *PLoS One*, vol. 8, no. 10, p. e76518, Jan. 2013.

[43] D. Iliopoulos, M. Lindahl-Allen, C. Polytarchou, H. A. Hirsch, P. N. Tsichlis, and K. Struhl, "Loss of miR-200 inhibition of Suz12 leads to polycomb-mediated repression required for the formation and maintenance of cancer stem cells.," *Mol. Cell*, vol. 39, no. 5, pp. 761–72, Sep. 2010.

[44] Y. Qiao, X. Jiang, S. T. Lee, R. K. M. Karuturi, S. C. Hooi, and Q. Yu, "FOXQ1 regulates epithelial-mesenchymal transition in human cancers.," *Cancer Res.*, vol. 71, no. 8, pp. 3076–86, Apr. 2011.

[45] M. T. E. Montales, O. M. Rahal, J. Kang, T. J. Rogers, R. L. Prior, X. Wu, and R. C. M. Simmen, "Repression of mammosphere formation of human breast cancer cells by soy isoflavone genistein and blueberry polyphenolic acids suggests diet-mediated targeting of cancer stem-like/progenitor cells.," *Carcinogenesis*, vol. 33, no. 3, pp. 652–60, Mar. 2012.

[46] S. Yin, L. Xu, S. Bandyopadhyay, S. Sethi, and K. B. Reddy, "Cisplatin and TRAIL enhance breast cancer stem cell death," *Int. J. Oncol.*, vol. 39, no. 4, pp. 891–898, Oct. 2011.

[47] Z. Du, J. Li, L. Wang, C. Bian, Q. Wang, L. Liao, X. Dou, X. Bian, and R. C. Zhao, "Overexpression of ΔNp63α induces a stem cell phenotype in MCF7 breast carcinoma cell line through the Notch pathway.," *Cancer Sci.*, vol. 101, no. 11, pp. 2417–24, Nov. 2010.

[48] F. Zhang, C. Song, Y. Ma, L. Tang, Y. Xu, and H. Wang, "Effect of fibroblasts on breast cancer cell mammosphere formation and regulation of stem cell-related gene expression," *Int. J. Mol. Med.*, vol. 28, no. 3, pp. 365–371, Sep. 2011.

[49] B. G. Debeb, W. Xu, H. Mok, L. Li, F. Robertson, N. T. Ueno, J. Reuben, A. Lucci, M. Cristofanilli, and W. A. Woodward, "Differential radiosensitizing effect of valproic acid in differentiation versus self-renewal promoting culture conditions.," *Int. J. Radiat. Oncol. Biol. Phys.*, vol. 76, no. 3, pp. 889–95, Mar. 2010.

[50] T. Brabletz, A. Jung, S. Spaderna, F. Hlubek, and T. Kirchner, “Opinion: migrating cancer stem cells - an integrated concept of malignant tumour progression.,” *Nat. Rev. Cancer*, vol. 5, no. 9, pp. 744–9, Sep. 2005.

[51] A. Giese, R. Bjerkvig, M. E. Berens, and M. Westphal, “Cost of migration: invasion of malignant gliomas and implications for treatment.,” *J. Clin. Oncol.*, vol. 21, no. 8, pp. 1624–36, Apr. 2003.

[52] W.-H. Su, P.-C. Chuang, E.-Y. Huang, and K. D. Yang, “Radiation-induced increase in cell migration and metastatic potential of cervical cancer cells operates via the K-Ras pathway.,” *Am. J. Pathol.*, vol. 180, no. 2, pp. 862–71, Feb. 2012.

[53] A. C. Pickhard, J. Margraf, A. Knopf, T. Stark, G. Piontek, C. Beck, A.-L. Boulesteix, E. Q. Scherer, S. Pigorsch, J. Schlegel, W. Arnold, and R. Reiter, “Inhibition of radiation induced migration of human head and neck squamous cell carcinoma cells by blocking of EGF receptor pathways.,” *BMC Cancer*, vol. 11, no. 1, p. 388, Jan. 2011.